Supporting Information for

"Recognizing the waveform of a foreshock"

Lippiello E.[1], **Petrillo G.**[1], **Godano C.** [1]

[1]Department of Mathematics and Physics, University of Campania "L. Vanvitelli", 81100 Caserta, Italy.

Corresponding author: E. Lippiello, eugenio.lippiello@unicampania.it

Index	Code Name	Mw	Date	Epicenter		Q	n_{obs}	$\delta\mu$
β								
1	Tohoku	7.3	2011/03/09	38.435 N 142.842 E	4.78	6	-6.51	0.39
2	Tohoku	9.1	2011/03/11	38.297 N 142.373 E	8.75E-6	17	-1.40	0.97
3	Iquique	6.7	2014/03/16	19.981 S 70.702 W	0.17	9	-4.85	0.73
4	Iquique	6.2	2014/03/23	19.690 S 70.854 W	1.15	1	-6.57	0.65
5	Iquique	8.1	2014/04/01	19.610 S 70.769 W	1.40E-4	21	-1.83	1.05
6	Karpathos	6.1	2015/04/16	35.189 N 26.824 E	5.09E-3	4	-3.30	0.56
7	Shikotan	6.3	2015/07/07	43.910 N 147.975 E	0	0	-6.38	1
8	Makurazaki	6.7	2015/11/13	31.001 N 128.873 E	1.96E-2	1	-4.25	1
9	Lefkada	6.5	2015/11/17	38.670 N 20.600 E	9.98E-3	2	-4.42	0.75
10	Shizunai	6.7	2016/01/14	41.972 N 142.781 E	0	-7.06	1	
11	Kumamoto	6.2	2016/04/14	32.788 N 130.704 E	0.18	17	-4.57	0.71
12	Kumamoto	7.0	2016/04/15	32.791 N 130.754 E	1.49E-3	21	-2.67	0.95
13	Miyako	6.0	2016/08/20	40.394 N 143.680 E	0	0 -5.58	0.60	
14	Amatrice	6.2	2016/08/24	42.723 N 13.188 E	8.84E-3	4	-3.83	0.69
15	Visso	6.1	2016/10/26	42.956 N 13.067 E	0.21	4	-4.57	0.82
16	Norcia	6.6	2016/10/30	42.862 N 13.096 E	5.02E-3	4	-3.67	0.91
17	Kurayoishi	6.6	2016/10/21	35.374 N 133.809 E	3.65E-3	3	-4.30	0.91
18	Ishinomaki	6.1	2016/11/11	38.497 N 141.566 E	0	0	-6.41	1
19	Namie	6.9	2016/11/21	37.393 N 141.387 E	3.08E-3	14	-3.29	0.95
20	Ferndale	6.6	2016/12/08	40.454 N 126.194 W	0	0 -6.41	1	
21	Valparaiso	6.0	2017/04/23	33.03 S 72.030 W	2.97	5	-5.76	0.69
22	Valparaiso	6.9	2017/04/24	33.038 S 72.062 W	9.47E-2	4	-4.90	0.95
23	Lesvos	6.4	2017/06/12	38.930 N 26.365 E	4.94E-2	3	-4.84	1.04
24	Kos	6.6	2017/07/20	36.929 N 27.414 E	5.87E-4	21	-2.2	1.2
25	Naze	6.0	2017/07/26	26.898 N 130.184 E	0	0	-4.91	1
26	Misawa	6.3	2018/01/24	41.103 N 142.432 E	0	0	-6.26	1
27	Hualien	6.2	2018/02/04	24.157 N 121.708 E	0.33	10	-5.18	0.43
28	Hualien	6.4	2018/02/06	24.134 N 121.659 E	5.89E-3	5	-4.01	0.65
29	Oregon	6.2	2018/08/22	43.564 N 127.717 W	0	0	-5.84	1
30	Tomakomai	6.7	2018/09/05	42.686 N 141.929 E	1.76E-2	5	-5.01	0.86
31	Port Hardy	6.5	2018/10/22	49.259 N 129.412 W	0.59	2	-4.65	0.75

32	Port Hardy	6.8	2018/10/22	49.335 N 129.289 W	0.46	5	-4.17	0.84
33	Zakynthos	6.8	2018/10/25	37.520 N 20.557 E	3.46E-4	10	-2.21	0.86
34	Nishinoomote	6.3	2019/01/08	30.587 N 131.044 E	0	0	-6.75	1
35	Tsuruoka	6.4	2019/06/18	38.639 N 139.477 E	4.81E-2	2.0	-5.32	0.78
36	Ridgecrest	6.4	2019/07/04	35.705 N 117.504 W	6.32E-2	5	-4.29	0.61
37	Ridgectest	7.0	2019/07/06	35.770 N 117.599 W	1.29E-2	27	-3.38	0.83
38	Bella Bella	6.2	2019/07/04	51.237 N 130.501 W	0	0	-4.41	0.70
39	Namie	6.3	2019/08/04	37.759 N 141.603 E	0	0	-6.96	1
40	Oregon	6.3	2019/08/29	43.543 N 127.882 W	0	0	-6.36	1
41	Albania	6.4	2019/11/26	41.514 N 19.526 E	1.54E-3	2	-3.42	0.98
42	Platanos	6.0	2019/11/27	35.717 N 23.228 E	0	0 -7.11	1	
43	Port Hardy	6.0	2019/12/23	50.607 N 129.937 W	10.41	7	-4.77	0.65
44	Port Hardy	6.0	2019/12/23	50.517 N 129.757 W	2.67	1	-5.73	0.65
45	Port Hardy	6.3	2019/12/25	50.611 N 129.963 W	0	0	-4.68	0.87
46	Idaho	6.5	2020/03/31	44.465 N 115.118 W	4.67E-4	1	-3.16	1.30
47	Ofunato	6.3	2020/04/19	38.895 N 142.005 E	0	0	-6.51	1

Table 1: List of earthquakes considered in the study. We highlight the Mw6.0+ foreshocks followed by a larger earthquake.

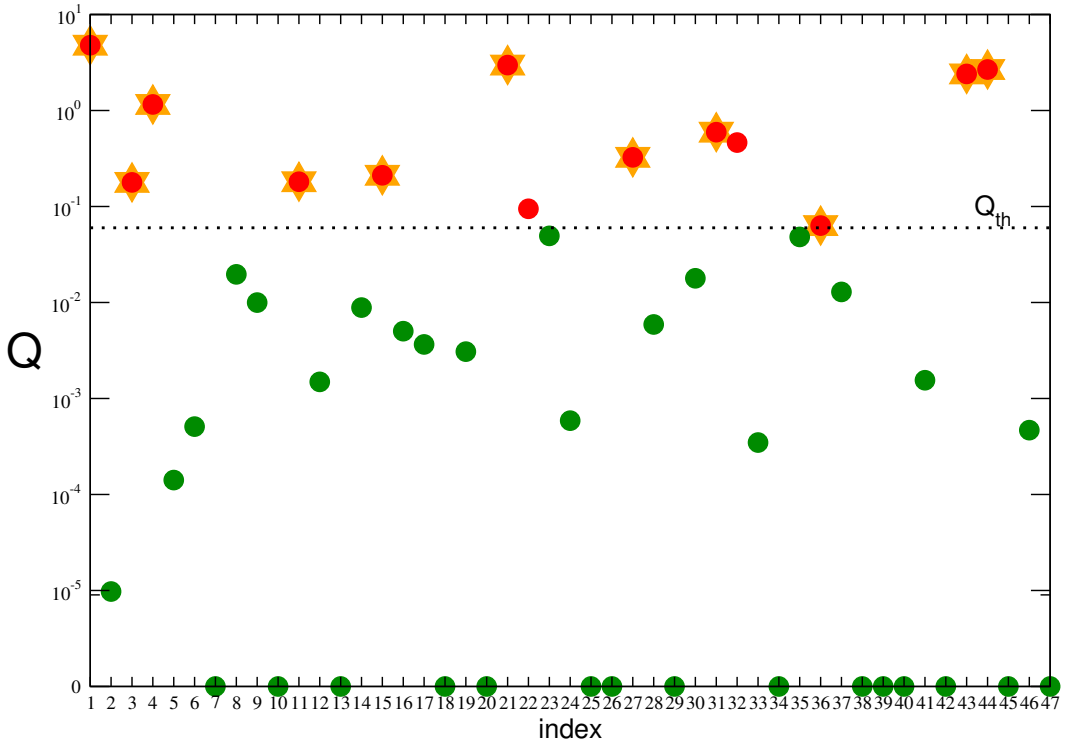

Figure 1: **A traffic light classification** We plot the Q value for each earthquake listed in Suppl. Table 1, according to the corresponing index in the Table. We use $\beta = 1$ in order to have a Q value available within 45 minutes after the earthquake. We identify a Q_{th} and earthquakes with $Q > Q_{th}$ switch the alarm on and are plotted in red. Events with $Q < Q_{th}$ should be not followed by a larger earthquake and are plotted in green. Yellow stars indicates the events effectively followed by a larger one within 10 days.

1 Comparison with the Gulia & Wiemer method

The Gulia & Wiemer (GW) method is based on the observation that in the large majority of aftershock sequences, the b value increases, typically more than the 20%, after a Mw6+ mainshock. Accordingly, a decrease in the b value must be interpreted as a signature of an anomalous behavior which increases the occurrence probability of a subsequent larger earthquake. The method is then based on the evaluation of the b value both in periods of stationary seismicity before each earthquake, b_{norm}, and in the temporal period after the big earthquake b_{after}.

The method presented in this study is based on the evaluation of the quantities μ_L, μ_B and n_{obs}, leading to $Q = n_{obs} \times 10^{-2\mu_L + \mu_B}$. The main difference with the GW is that the

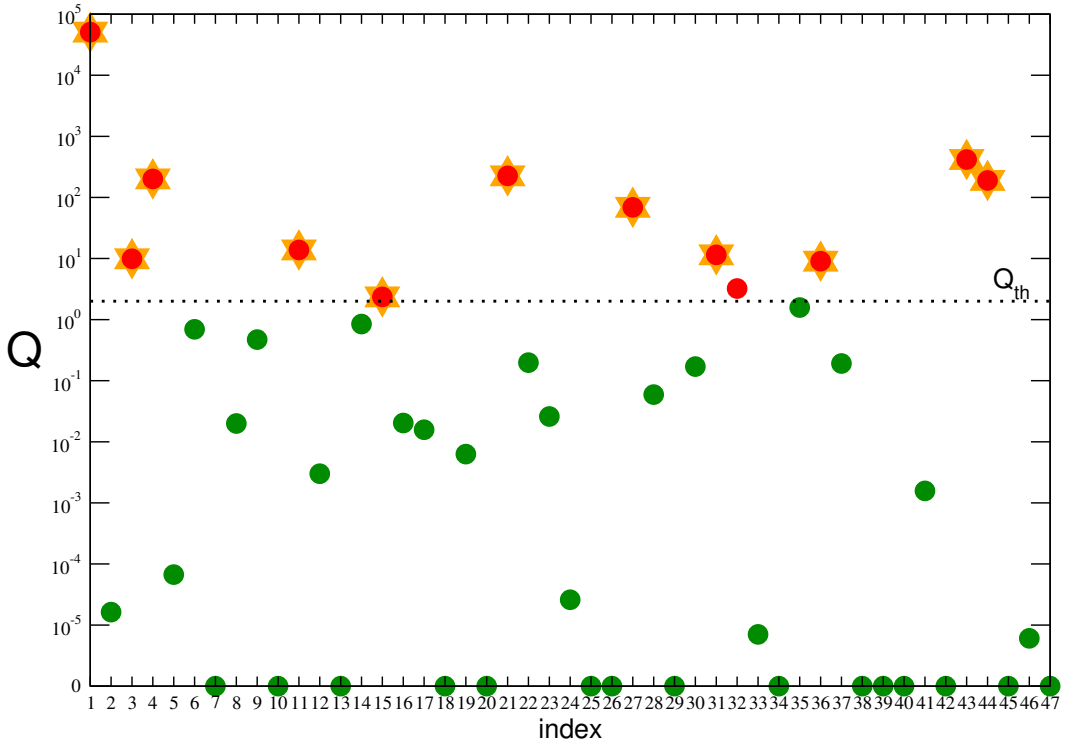

Figure 2: **A traffic light classification including** β The same of Supp. Fig.1 but implementing in the definition of Q the value of β extracted from data. The only false alert is for the Mw6.8 Port Hardy of 2018 which occurred only 37 minutes after the Mw6.5 foreshock.

quantity Q can be obtained directly from the envelope $\mu(t)$ and this leads to several advantages with respect to the GW method:

- The GW method is strongly affected by the fact that many aftershocks are hidden by coda waves of previuos larger events and cannot be identified. For this reason, the evaluation of b_{after} can start only after an exclusion period which depends on the quality of the seismic network. Furthermore the precise interval to consider is an experts choice and this does not allow one to implement this method in an automatic procedure. Conversely, the quantity Q can be measured in real-time in an automatic way and this information could be concretely available within a temporal interval smaller than 1 hour after each earthquake;
- The GW method needs very accurate seismic natwork able to detect and process Mw2+ events almost in real time in temporal periods with a huge seismic activity as the ones following Mw6+ earthquakes. This implies that the earthquake must occur in areas with excellent network coverage and with very efficient automatic routines for event location. Only very few seismic networks satisfy these conditions. Conversely, for the evaluation of Q it is sufficient that the earthquake is recorded by just one station which must present a sufficiently low level of $\mu_B \lesssim 1$ and must be sufficiently close to produce a perceived magnitude $\mu_M \geq 5$;
- In the GW it is important to achieve relative hypocentre accuracies of about ~ 1 km. In the evaluation of Q only an indicative position of the epicenter is necessary in order to choose the closest in space seismic station.

An important remark, already stated in the manuscript, is that the two methods are not alternative and their combined use can significantly improve their individual forecasting efficiencies.

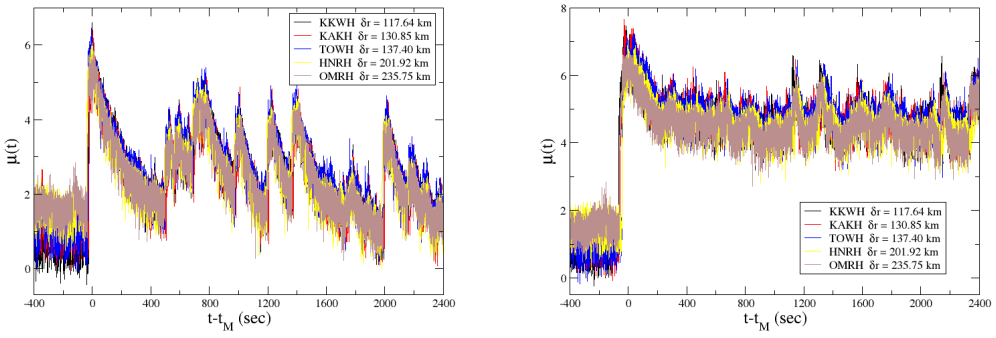

Figure 3: **The envelope function of the Tohoku sequence.** In the left panel we plot the envelope function after the Mw7.3 Tohoku foreshock and in the right panel we plot the envelope function after the Mw9.1 Tohoku mainshock. Different colors correspond to the signal recorded at seismic stations with different epicental distance δr from the epicenter (see the legend).

2 Details on the considered earthquakes

2.1 TOHOKU 2011/03/09 - 2011/03/11

The estimated slip distribution of the largest foreshock (Mw7.3) suggests that it did not rupture the fault of the Mw9.1 mainshock occurred on 11 March 2011. Indeed the epicenter of the mainshock is located adjacent to the southern termination of the foreshock slip distribution. This indicates that highly resistive patch around the epicenter of the mainshock was able to withstand the stress caused by the largest foreshock. Stress increases larger than 0.1 bars commonly raise regional seismicity and thus potentially bring a major fault to failure with delays ranging from seconds to decades. The Coulomb stress change on thrust faults with the same geometry as the largest foreshock amounts to 1.6-4.5 bars within a 4 km radius of the hypocenter of the mainshock (depth = 23.7 km). Whereas, at the hypocenter, the stress increased by 3.5 bars. This suggests that the Mw9.1 Tohoku earthquake was brought closer to failure by the largest foreshock. The foreshocks occurred on 9 March 2011 were mostly located on the upper part of the major slip region of the largest foreshock migrating toward the epicenter of the mainshock. The foreshock migration was interpreted as propagation of slow slip by Kato et al. [2012], the slow slip also increased the static stress on the plate interface in ad-

dition to that by the largest foreshock. These static stress increases might have finally brought the 2011 Tohoku earthquake to failure.

REFERENCES

Aditya Riadi Gusman, Mitsuteru Fukuoka, Yuichiro Tanioka, and Shinichi Sakai Effect of the largest foreshock (Mw7.3) on triggering the 2011 Tohoku earthquake (Mw9.0) GEOPHYSICAL RESEARCH LETTERS, VOL. 40, 497500, doi:10.1002/grl.50153, 2013

Kato, A., K. Obara, T. Igarashi, H. Tsuruoka, S. Nakagawa, and N. Hirata (2012), Propagation of Slow Slip Leading Up to the 2011 Mw 9.0 Tohoku-Oki Earthquake, Science, 335(6069), 705708, doi:10.1126/science.1215141.

Table 2: W-phase Moment Tensor for Tohoku foreshock

Moment	$9.809E19$ N-m
Magnitude	7.26 Mw
Depth	19.5 km
Half duration	13.00 sec

	Strike	**Dip**	**Rake**
NP1	185°	16°	68°
NP2	28°	75°	96°

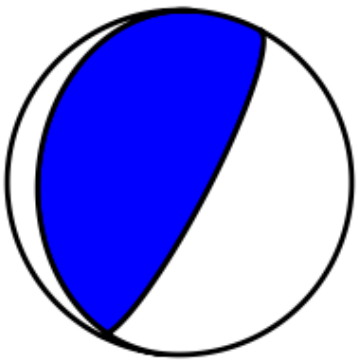

Figure 4: Beach ball for Tohoku foreshock.

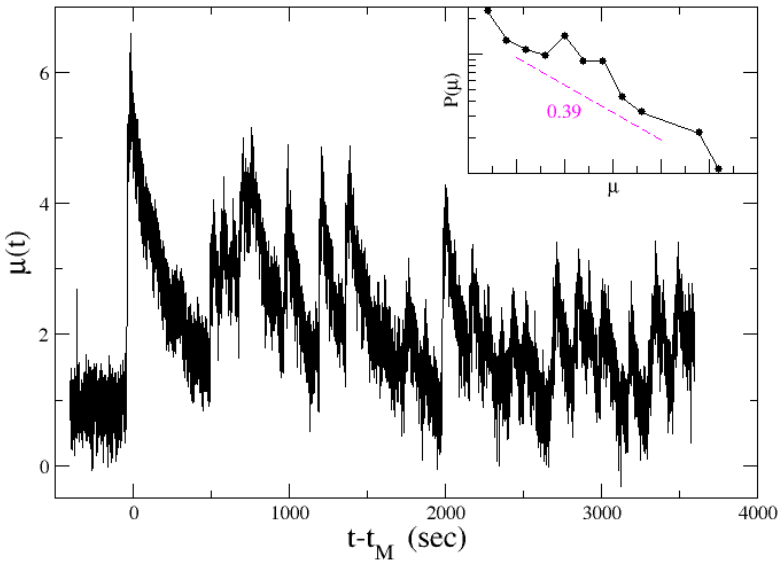

Figure 5: In main panel we plot the envelope function after the Mw7.3 Tohoku foreshock. (Inset) Distribution of the percieved magnitude $P(\mu)$ calculated considering all aftershocks with percieved magnitude $\mu = \mu_M - 3$ in a 24-hours time window after the mainshock occurrence.

Table 3: W-phase Moment Tensor for Tohoku mainshock

Moment	$5.593E22$ N-m
Magnitude	9.10 Mw
Depth	11.5 km
Half duration	73.00 sec

	Strike	**Dip**	**Rake**
NP1	193°	9°	78°
NP2	25°	81°	92°

The network and the name of the considered seismic station is N.KAKH at coordinates 38.5158N, 141.3421E at altitude 5 m with sampling frequency of 100 Hz.

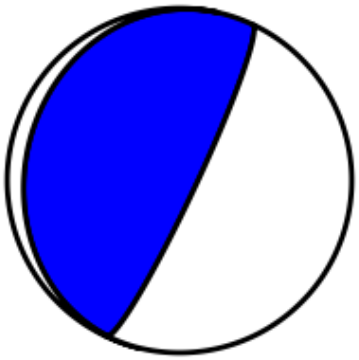

Figure 6: Beach ball for Tohoku mainshock

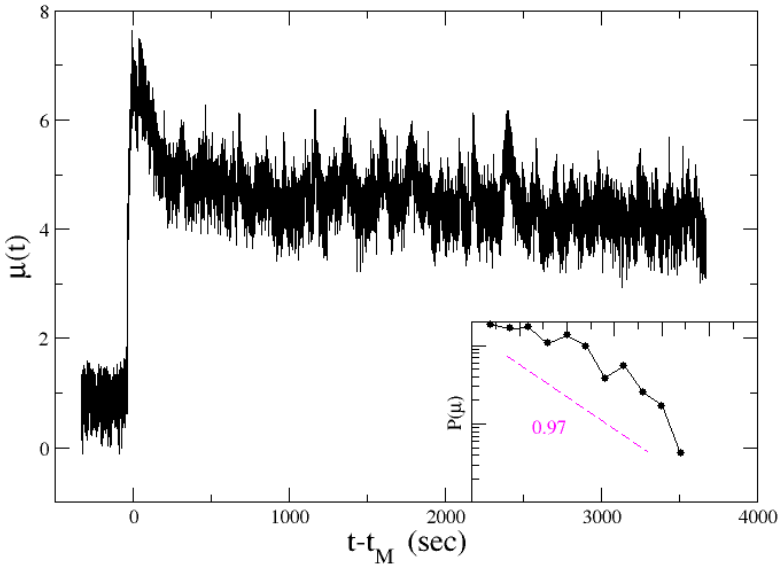

Figure 7: In main panel we plot the envelope function after the Mw9.1 Tohoku mainshock. (Inset) Distribution of the percieved magnitude $P(\mu)$ calculated considering all aftershocks with percieved magnitude $\mu = \mu_M - 3$ in a 24-hours time window after the mainshock occurrence.

2.2 IQUIQUE 2014/03/16 - 2014/03/23 - 2014/04/01

Herman et al. (2016) showed the complex dynamics leading to the occurrence of the Mw8.2 mainshock. After the initial Mw6.7 event, a Mw6.4 earthquake occurred at the border of the Mw6.7 fault. The following Mw6.2 event occurred in a zone of increased Coulomb stress. Then a series of Mw5.5 events occurred on the fault area of the subsequent mainshock. The region of greatest slip generated by the mainshock has essentially no correlation with either the foreshock positive stress change or with the location of the foreshocks themselves. Indeed the main slip patch of the April 1st earthquake extends farther downdip into a segment of the interface unaffected by the foreshock stress changes, suggesting that the down-dip part of the system was loaded by a mechanism other than the foreshock sequence. Moreover a slow slip mechanism have to be added to the increased Coulomb stress in order to have a good fit of the deformation field (Kato and Nakagawa, 2014; Ruitz et al., 2014; Bedford et al, 2015). This slow slip can be associated to the foreshock occurrence or, alternatively, interpreted as independent of their occurrence. In both the scenarios this slow slip generates an increase of Coulomb stress in the area of the mainshock fault (Herman et al., 2016).

REFERENCES

M. W. Herman, K. P. Furlong, G. P. Hayes and H. M. Benz Foreshock triggering of the 1 April 2014 Mw8.2 Iquique, Chile, earthquake Earth and Planetary Science Letters 447 (2016) 119129

Table 4: W-phase Moment Tensor for Iquique 1

Moment	$1.591E19$ N-m
Magnitude	6.73 Mw
Depth	15.5 km
Half duration	– sec

	Strike	**Dip**	**Rake**
NP1	277°	18°	63°
NP2	126°	74°	98°

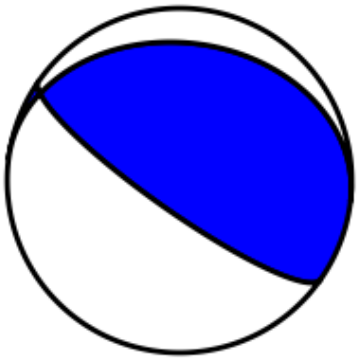

Figure 8: Beach ball for Iquique 1

Table 5: W-phase Moment Tensor for Iquique 2

Moment	$3.281E18$ N-m
Magnitude	6.28 Mw
Depth	23.5 km
Half duration	– sec

	Strike	**Dip**	**Rake**
NP1	347°	22°	105°
NP2	151°	69°	84°

Table 6: W-phase Moment Tensor for Iquique 3

Moment	$2.348E21$ N-m
Magnitude	8.18 Mw
Depth	25.5 km
Half duration	– sec

	Strike	**Dip**	**Rake**
NP1	358°	12°	107°
NP2	161°	79°	87°

The network and the name of the considered seismic station is CX.PSGCX at coordinates 19.5972S, 70.1230O at altitude 966 m with sampling frequency of 100 Hz.

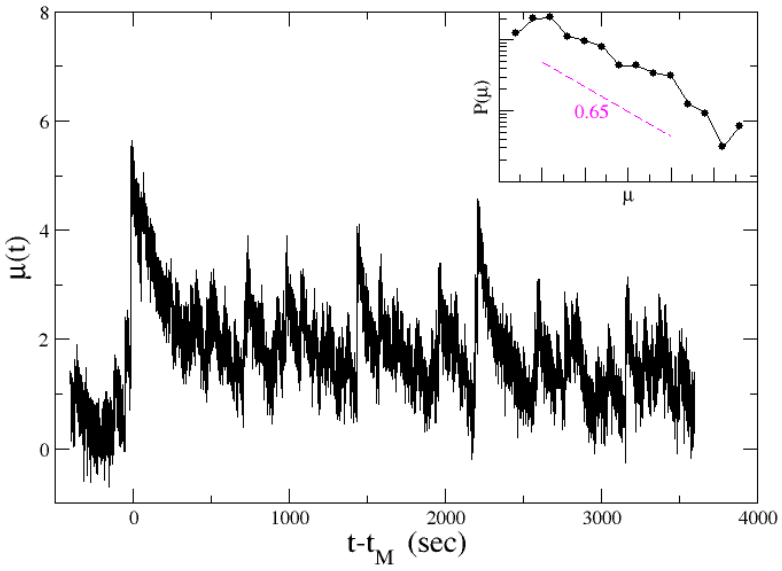

Figure 9: In main panel we plot the envelope function after the Mw6.7 Iquique foreshock. (Inset) Distribution of the percieved magnitude $P(\mu)$ calculated considering all aftershocks with percieved magnitude $\mu = \mu_M - 3$ in a 24-hours time window after the mainshock occurrence.

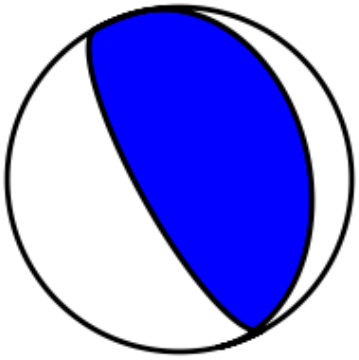

Figure 10: Beach ball for Iquique 2

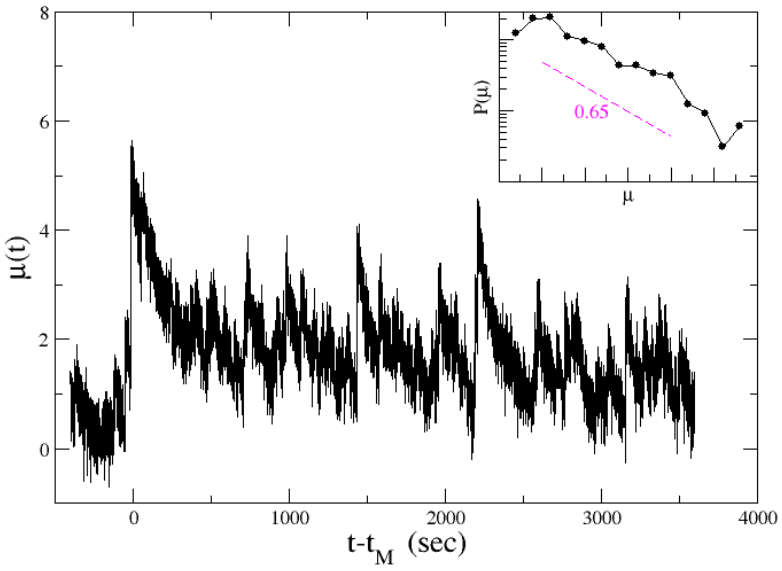

Figure 11: In main panel we plot the envelope function after the Mw6.2 Iquique foreshock. (Inset) Distribution of the percieved magnitude $P(\mu)$ calculated considering all aftershocks with percieved magnitude $\mu = \mu_M - 3$ in a 24-hours time window after the mainshock occurrence.

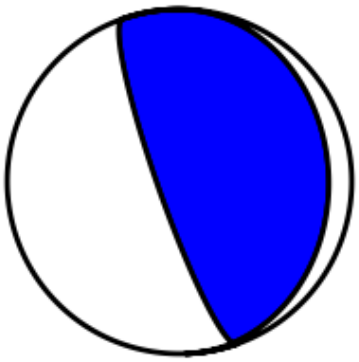

Figure 12: Beach ball for Iquique mainshok

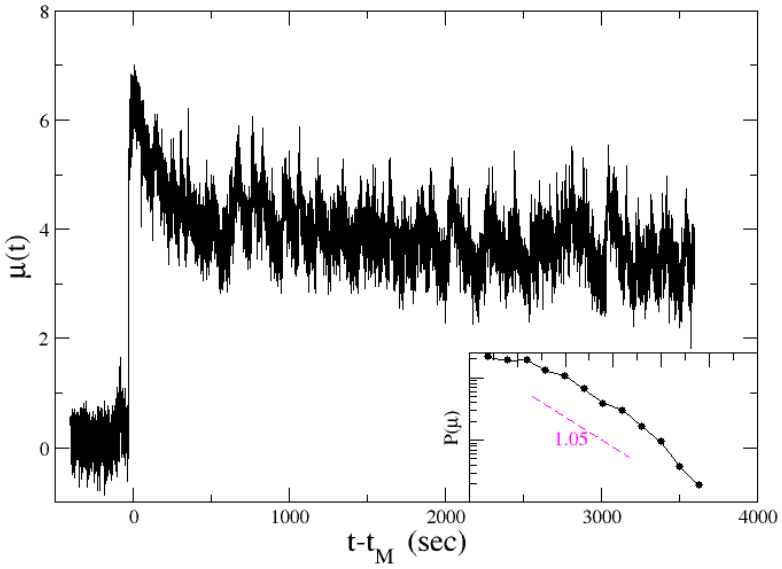

Figure 13: In main panel we plot the envelope function after the Mw8.1 Iquique mainshock. (Inset) Distribution of the percieved magnitude $P(\mu)$ calculated considering all aftershocks with percieved magnitude $\mu = \mu_M - 3$ in a 24-hours time window after the mainshock occurrence.

2.3 KARPATHOS 2015/04/16

On 16 April 2015 a Mw6.0 earthquake occurred at 49 km SW of Karpathos, Greece. The event occurred at a depth of about 30 km.

Table 7: W-phase Moment Tensor for Karpathos

Moment	$1.456E18$ N-m
Magnitude	6.04 Mw
Depth	30.5 km
Half duration	– sec

	Strike	**Dip**	**Rake**
NP1	293°	54°	142°
NP2	47°	60°	43°

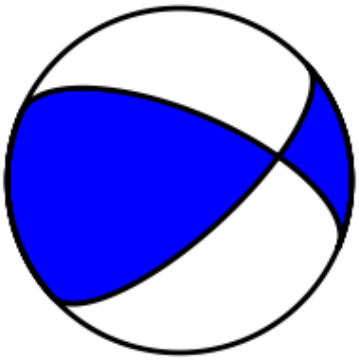

Figure 14: Beach ball for Karpathos

The network and the name of the considered seismic station is HL.KARP at coordinates 35.5471N, 27.1611E at altitude 524 m with sampling frequency of 100 Hz.

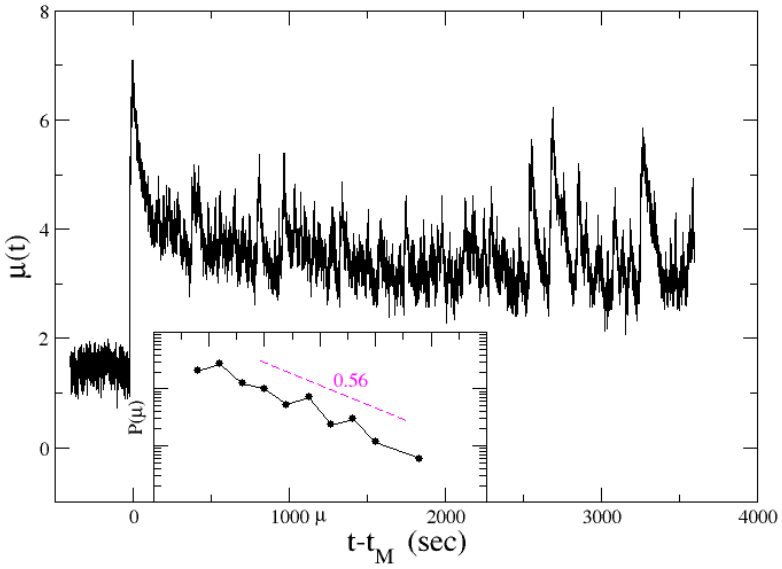

Figure 15: In main panel we plot the envelope function after the Karpathos mainshock. (Inset) Distribution of the percieved magnitude $P(\mu)$ calculated considering all aftershocks with percieved magnitude $\mu = \mu_M - 3$ in a 24-hours time window after the mainshock occurrence.

2.4 SHIKOTAN 2015/07/07

A Mw6.3 earthquake struck 101 km E of Shikotan, Japan. The event occurred of a depth of about 60 km.

Table 8: W-phase Moment Tensor for Shikotan

Moment	$3.547E18$ N-m
Magnitude	6.30 Mw
Depth	60.5 km
Half duration	– sec

	Strike	**Dip**	**Rake**
NP1	171°	24°	40°
NP2	43°	75°	109°

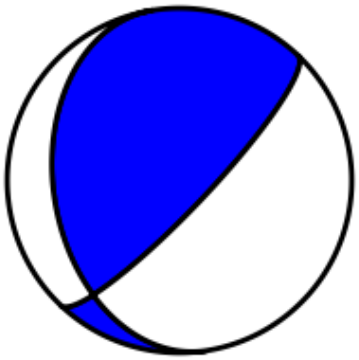

Figure 16: Beach ball for Shikotan

The network and the name of the considered seismic station is N.NMRF at coordinates 43.3673N, 145.7379E at altitude 20 m with sampling frequency of 100 Hz.

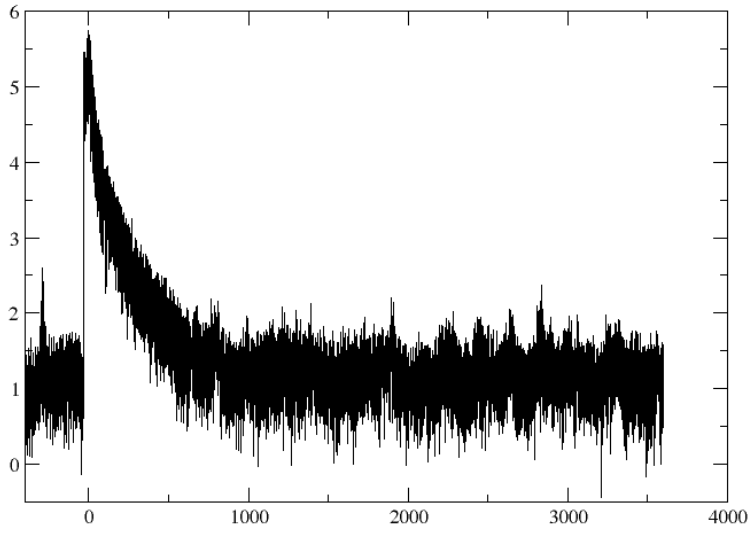

Figure 17: In main panel we plot the envelope function after the Shikotan mainshock. We do not plot the distribution of the percieved magnitude $P(\mu)$ because we find only a small number of aftershocks with percieved magnitude $\mu = \mu_M - 3$ in a 24-hours time window after the mainshock occurrence.

2.5 MAKURAZAKI 2015/11/13

A Mw6.7 earthquake has struck off the south-western coast of Japan. The event occurred at a depth of about 10 km.

Table 9: W-phase Moment Tensor for Makurazaki

Moment	$1.605E19$ N-m
Magnitude	6.74 Mw
Depth	23.5 km
Half duration	13.00 sec

	Strike	**Dip**	**Rake**
NP1	190°	85°	−170°
NP2	99°	80°	−5°

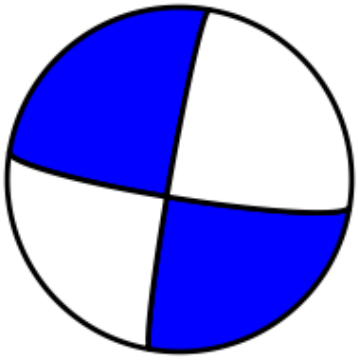

Figure 18: Beach ball for Makurazaki

The network and the name of the considered seismic station is N.CRNH at coordinates 31.3741N, 130.4333E at altitude 119 m with sampling frequency of 100 Hz.

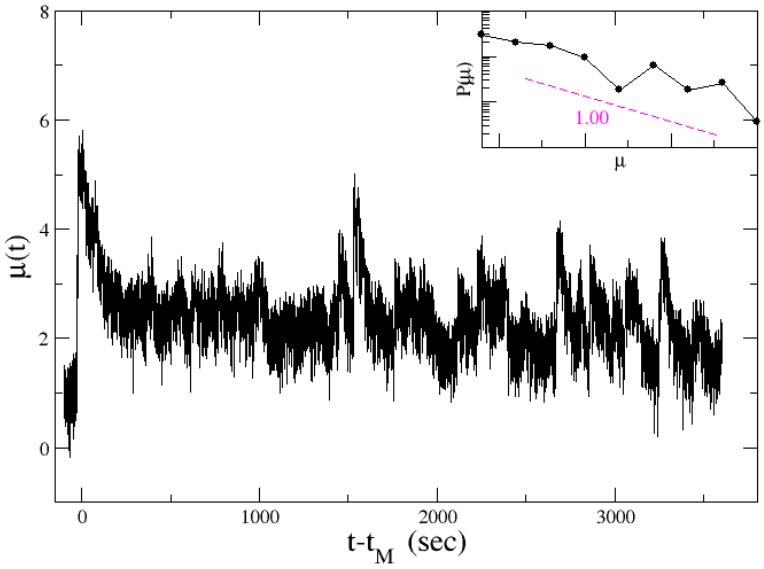

Figure 19: In main panel we plot the envelope function after the Makurazaki mainshock. (Inset) Distribution of the percieved magnitude $P(\mu)$ calculated considering all aftershocks with percieved magnitude $\mu = \mu_M - 3$ in a 24-hours time window after the mainshock occurrence.

2.6 LEFKADA 2015/11/17

The Mw6.5 earthquake accomodates right-lateral strike slip motion. It has got the largest reported magnitude for earthquakes in Lefkada island. The activity took place and produced damage along the southwestern shoreline and is associated with the southern branch of Lefkada Fault Zone. The rupture reflects the right-lateral strike-slip motion that takes place along the KTFZ, the major fault zone of the central Ionian Islands area where four strong earthquakes occurred in $\sim$ 12 years. The aftershock distribution reveals that the main slip is associated with a fault of about 17 km long, smaller than predicted from scaling laws, along the southwestern coast of Lefkada Island. The focal mechanisms calculated for 36 aftershocks with Mw$\geq$3.3 exhibit predominantly strike slip motion, and reflect local details of the stress pattern. Some of these mechanisms are different than the one of the main shock, manifesting motion on faults with different characteristics. The distribution of aftershocks implies static stress transfer to secondary faults accommodating deformation during the activation of the main faults in a fault population. Positive static stress changes were calculated at the aftershock hypocentral locations of the adjacent to the main rupture northern and southern clusters.

REFERENCES

Papadimitriou, E., Karakostas, V., Mesimeri, M. et al. The Mw6.5 17 November 2015 Lefkada (Greece) Earthquake: Structural Interpretation by Means of the Aftershock Analysis. Pure Appl. Geophys. 174, 38693888 (2017). https://doi.org/10.1007/s00024-017-1601-3

Table 10: W-phase Moment Tensor for Lefkada

Moment	$6.227E18$ N-m
Magnitude	6.46 Mw
Depth	11.5 km
Half duration	6.60 sec

	Strike	**Dip**	**Rake**
NP1	21°	85°	155°
NP2	113°	65°	6°

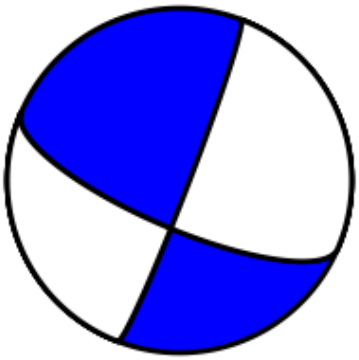

Figure 20: Beach ball for Lefkada

The network and the name of the considered seismic station is HT.PSDA at coordinates 38.114N, 20.5841E at altitude 48 m with sampling frequency of 100 Hz.

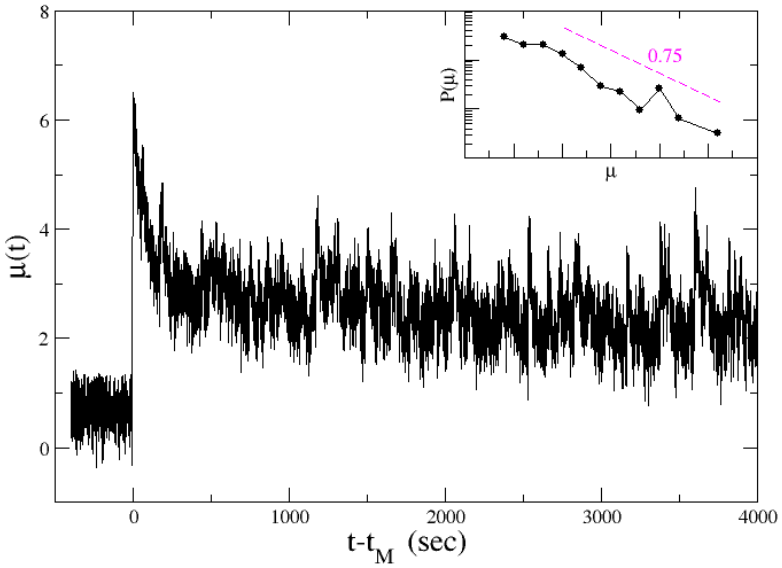

Figure 21: In main panel we plot the envelope function after the Lefkada mainshock. (Inset) Distribution of the percieved magnitude $P(\mu)$ calculated considering all aftershocks with percieved magnitude $\mu = \mu_M - 3$ in a 24-hours time window after the mainshock occurrence.

2.7 SHIZUNAI 2016/01/14

On 14 January 2016 a Mw6.7 earthquake occurred in the southeast of Japan's northen island of Hokkaido. The event was located 51 km southeast of the city of Shizunai.

Table 11: W-phase Moment Tensor for Shizunai

Moment	$1.343E19$ N-m
Magnitude	6.69 Mw
Depth	50.5 km
Half duration	3.00 sec

	Strike	**Dip**	**Rake**
NP1	216°	20°	107°
NP2	18°	71°	84°

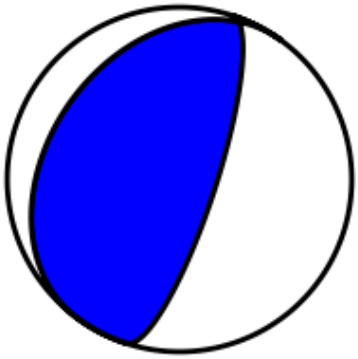

Figure 22: Beach ball for Shizunai

The network and the name of the considered seismic station is N.SAMH at coordinates 42.1330N, 142.9164E at altitude 40 m with sampling frequency of 100 Hz.

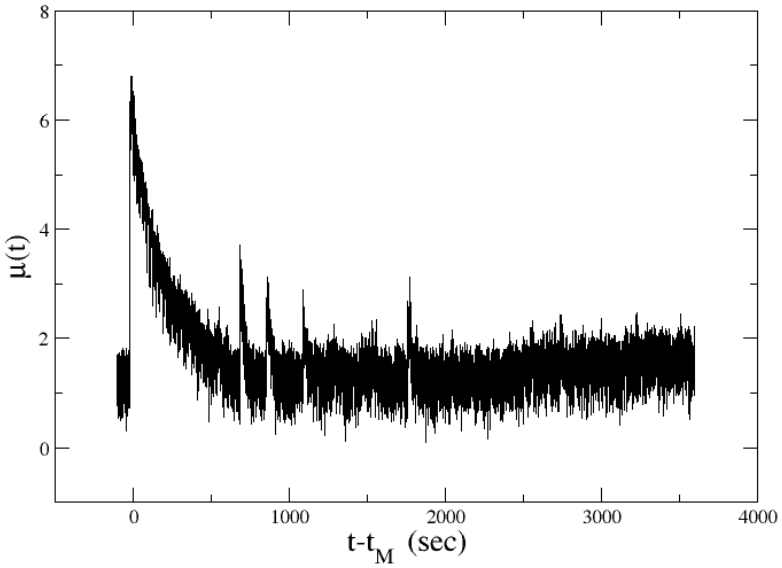

Figure 23: In main panel we plot the envelope function after the Shizunai mainshock. (Inset) Distribution of the percieved magnitude $P(\mu)$ calculated considering all aftershocks with percieved magnitude $\mu = \mu_M - 3$ in a 24-hours time window after the mainshock occurrence.

2.8 KUMAMOTO 2016/04/14 - 2016/04/15

Kato et al. (2016) relocated aftershocks showing as the foreshocks and the mainshock occurred on different fault planes. The first ones occurred on a subvertical hidden or blind fault plane, whereas the second occurred on a NW dipping fault plane (Yue et al. 2017). They also observed a downdip migration of foreshock activity, probably related to the initiation of the mainshock. The multiple point sources inversion indicates that the first foreshock (Mw = 6.2) is composed by three subevents: the first subevent was east dipping and was followed by two west dipping subevents (Shi et al., 2016).

REFERENCES

Kato, A., Fukuda, J. I., Nakagawa, S., Obara, K. (2016). Foreshock migration preceding the 2016 M w 7.0 Kumamoto earthquake, Japan. Geophysical Research Letters, 43, 89458953. https://doi.org/10.1002/2016GL070079

Shi, Q., Wei, S., Lindsey, E., Feng, L., Wang, T., Wang, Y., ... Hill, E. (2016). The 2016 Kumamoto earthquake sequence: A series of cross-fault and in-fault triggering events. Abstract S21A-2680 Presented at the 2016 AGU Fall Meeting, San Francisco, CA.

Yue, H., Ross, Z. E., Liang, C., Michel, S., Fattahi, H., Fielding, E., ... Jia, B. (2017). The 2016 Kumamoto M w = 7.0 earthquake: A significant event in a faultvolcano system. Journal of Geophysical Research: Solid Earth, 122, 91669183. https://doi.org/10.1002/ 2017JB014525

Table 12: W-phase Moment Tensor for Kumamoto 1

Moment	$2.153E18$ N-m
Magnitude	6.16 Mw
Depth	13.5 km
Half duration	5.00 sec

	Strike	**Dip**	**Rake**
NP1	303°	74°	9°
NP2	210°	81°	164°

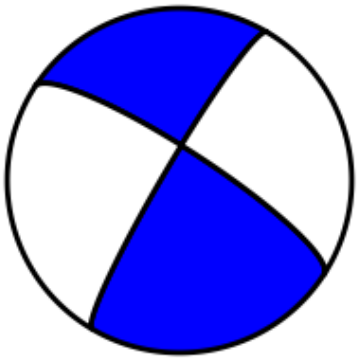

Figure 24: Beach ball for Kumamoto 1

Table 13: W-phase Moment Tensor for Kumamoto 2

Moment	$4.655E19$ N-m
Magnitude	7.05 Mw
Depth	17.5 km
Half duration	10.00 sec

	Strike	**Dip**	**Rake**
NP1	$224°$	$66°$	$-152°$
NP2	$122°$	$64°$	$-27°$

The network and the name of the considered seismic station is JP.JNU at coordinates 33.125N, 130.8766E at altitude 540 m with sampling frequency of 20 Hz.

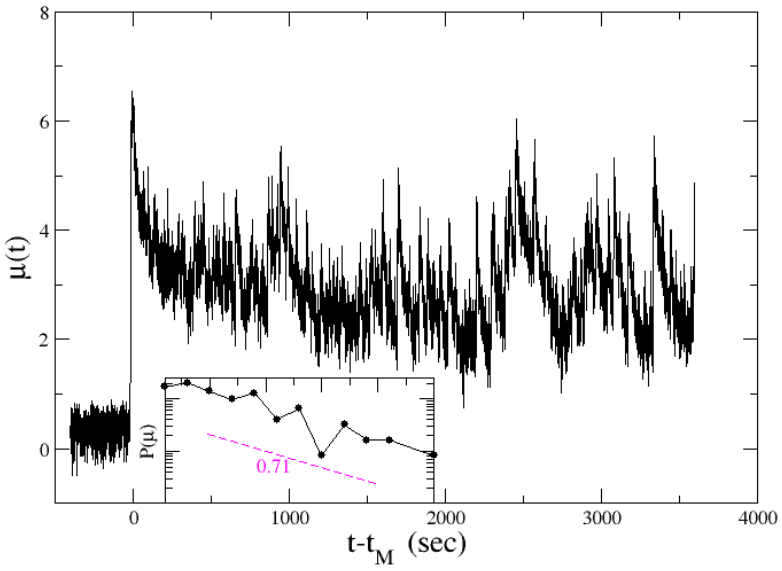

Figure 25: In main panel we plot the envelope function after the Mw6.2 Kumamoto foreshock. (Inset) Distribution of the percieved magnitude $P(\mu)$ calculated considering all aftershocks with percieved magnitude $\mu = \mu_M - 3$ in a 24-hours time window after the mainshock occurrence.

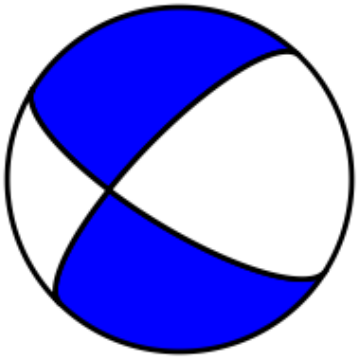

Figure 26: Beach ball for Kumamoto mainshock

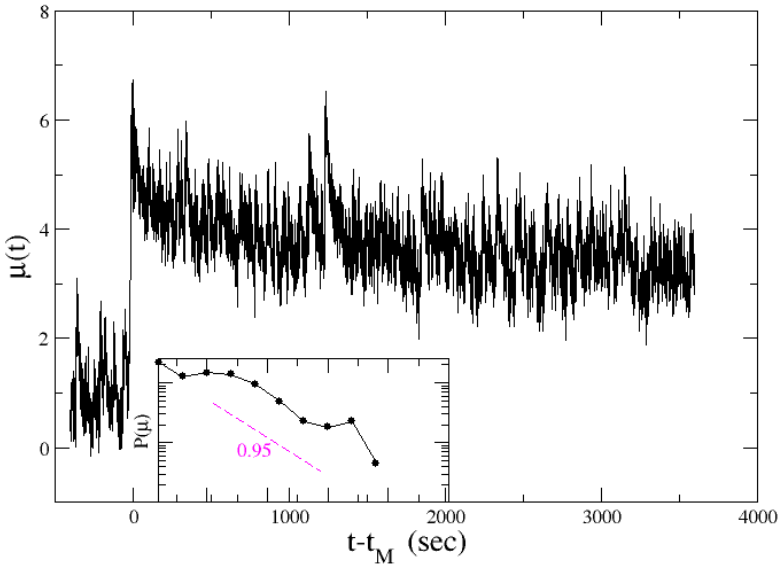

Figure 27: In main panel we plot the envelope function after the Mw7.0 Kumamoto mainshock. (Inset) Distribution of the percieved magnitude $P(\mu)$ calculated considering all aftershocks with percieved magnitude $\mu = \mu_M - 3$ in a 24-hours time window after the mainshock occurrence.

2.9 MIYAKO 2016/08/20

A Mw6.0 earthquake occurred off the east coast of Honshu, Japan. The depth is about 12 km. The epicenter was located approximately 169 km ENE of Miyako, Japan.

Table 14: W-phase Moment Tensor for Miyako

Moment	$1.328E18$ N-m
Magnitude	6.02 Mw
Depth	11.5 km
Half duration	7.00 sec

	Strike	**Dip**	**Rake**
NP1	197°	13°	91°
NP2	17°	77°	90°

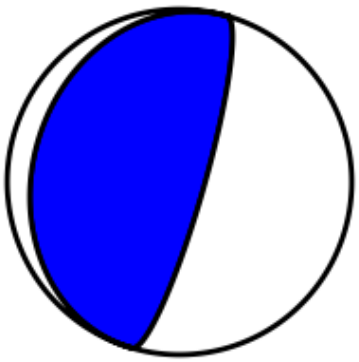

Figure 28: Beach ball for Miyako

The network and the name of the considered seismic station is N.TROH at coordinates 39.7435N, 141.9087E at altitude 200 m with sampling frequency of 100 Hz.

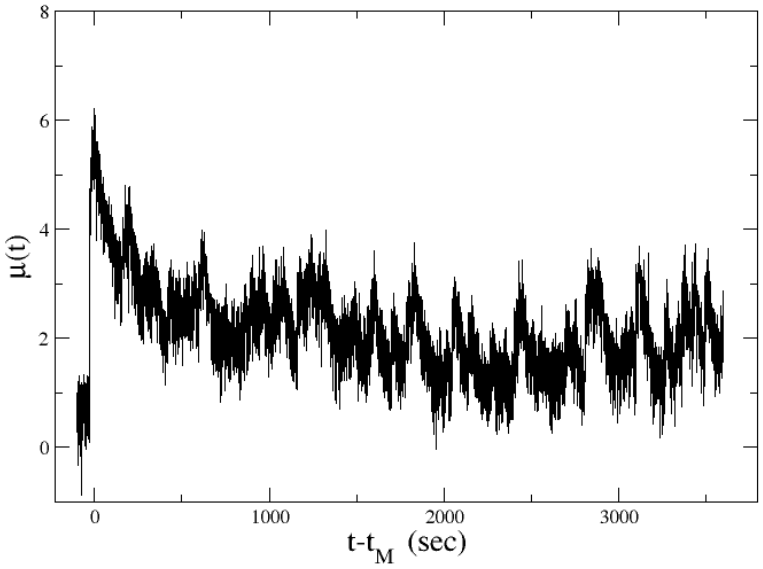

Figure 29: In main panel we plot the envelope function after the Miyako mainshock. We do not plot the distribution of the percieved magnitude $P(\mu)$ because we find only a small number of aftershocks with percieved magnitude $\mu = \mu_M - 3$ in a 24-hours time window after the mainshock occurrence

2.10 AMATRICE-VISSO-NORCIA 2016/08/24 - 2016/10/26 - 2016/10/30

The occurrence central Italy seismic sequence starting with the Amatrice earthquake on 24 August 2016 accelerated the occurrence of the 30 October Norcia earthquake (Mw6.6), but limited its magnitude by inhibiting the rupture on large portions of the fault plane. The preceding events hastened the mainshock and determined its features generating a patch of concentrated stress where, during the Norcia earthquake, the coseismic slip remained substantially confined. The rupture associated with the Amatrice earthquake (Mw6.2) started 18 km south of the hypocenter of the Norcia earthquake and propagated northward. Its occurrence induced, on the Norcia fault plane, significant Coulomb stress changes inhibiting the rupture on the southern half of the plane and slightly increasing the stress elsewhere. The aftershocks of this first earthquake were mainly peripheral to the reduced Coulomb stress area. The subsequent Mw7.1 Visso earthquake occurred in the area of increased coseismic stress and in the direction of higher dynamic strain causing a strong stress decrease on the northern part of the Norcia fault. Again the aftershocks mainly concentrated at the border of the decreased stress area, with no events in the central segment of the fault. This dynamics shaped a well defined area of concentrated stress with no seismic events inside and bordered by clusters of aftershock hypocenters distributed along a roughly annular zone where the Norcia earthquake will occur.

REFERENCES N.A. Pino, V. Convertito and R. Madariaga Clock advance and magnitude limitation through fault interaction: the case of the 2016 central Italy earthquake sequence Scientific Reports (2019) 9:5005 — https://doi.org/10.1038/s41598-019-41453-1

Table 15: W-phase Moment Tensor for Amatrice

[b]

Moment	$2.450E18$ N-m
Magnitude	6.19 Mw
Depth	11.5 km
Half duration	6.00 sec

	Strike	**Dip**	**Rake**
NP1	328°	43°	−103°
NP2	165°	49°	−78°

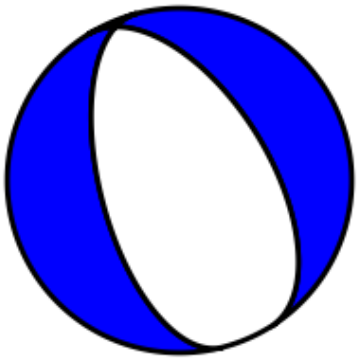

Figure 30: Beach ball for Amatrice

Table 16: W-phase Moment Tensor for Visso

Moment	$1.840E18$ N-m
Magnitude	6.11 Mw
Depth	11.5 km
Half duration	4.00 sec

	Strike	**Dip**	**Rake**
NP1	333°	40°	−92°
NP2	155°	50°	−89°

Table 17: W-phase Moment Tensor for Norcia

Moment	$1.071E19$ N-m
Magnitude	6.62 Mw
Depth	15.5 km
Half duration	7.20 sec

	Strike	**Dip**	**Rake**
NP1	162°	27°	−84°
NP2	335°	63°	−93°

The network and the name of the considered seismic station is MN.AQU at coordinates 42.354N, 13.405E at altitude 710 m with sampling frequency of 20 Hz.

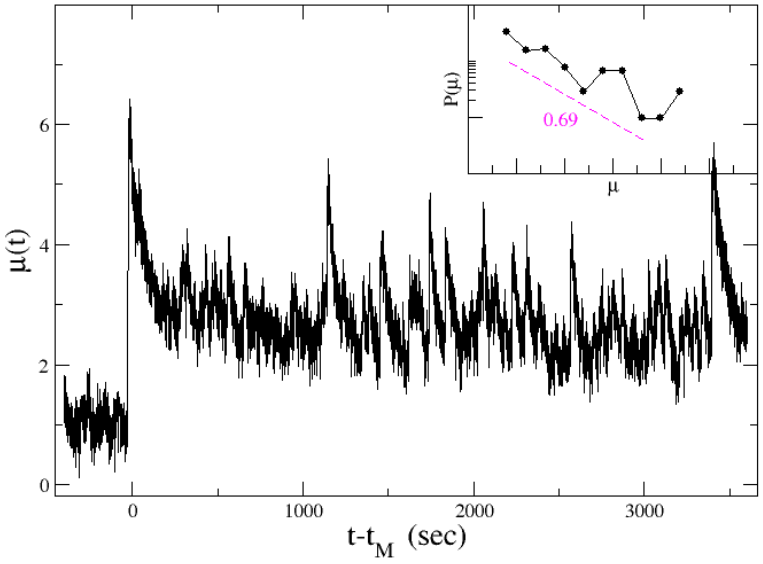

Figure 31: In main panel we plot the envelope function after the Mw6.2 Amatrice event. (Inset) Distribution of the percieved magnitude $P(\mu)$ calculated considering all aftershocks with percieved magnitude $\mu = \mu_M - 3$ in a 24-hours time window after the mainshock occurrence.

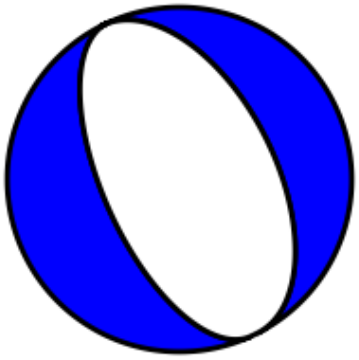

Figure 32: Beach ball for Visso

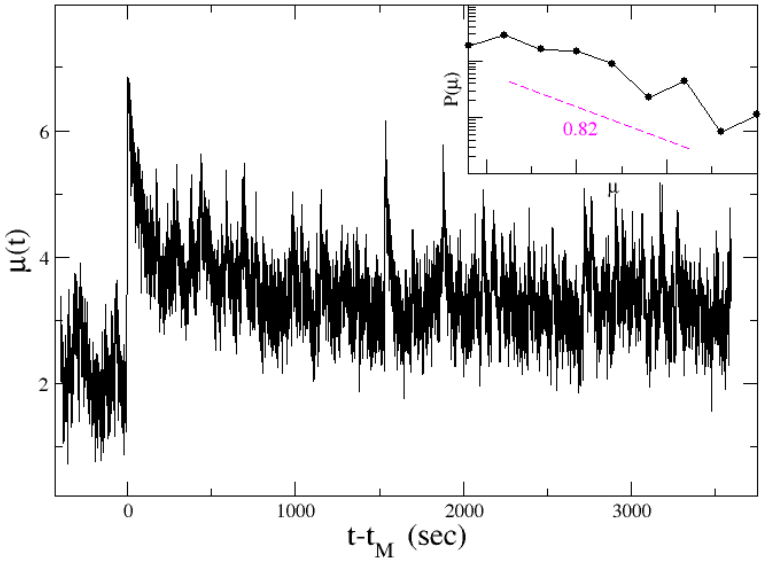

Figure 33: In main panel we plot the envelope function after the Mw6.1 Visso event. (Inset) Distribution of the percieved magnitude $P(\mu)$ calculated considering all aftershocks with percieved magnitude $\mu = \mu_M - 3$ in a 24-hours time window after the mainshock occurrence.

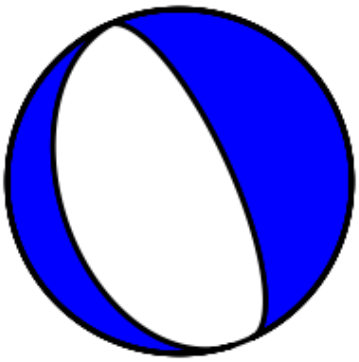

Figure 34: Beach ball for Norcia

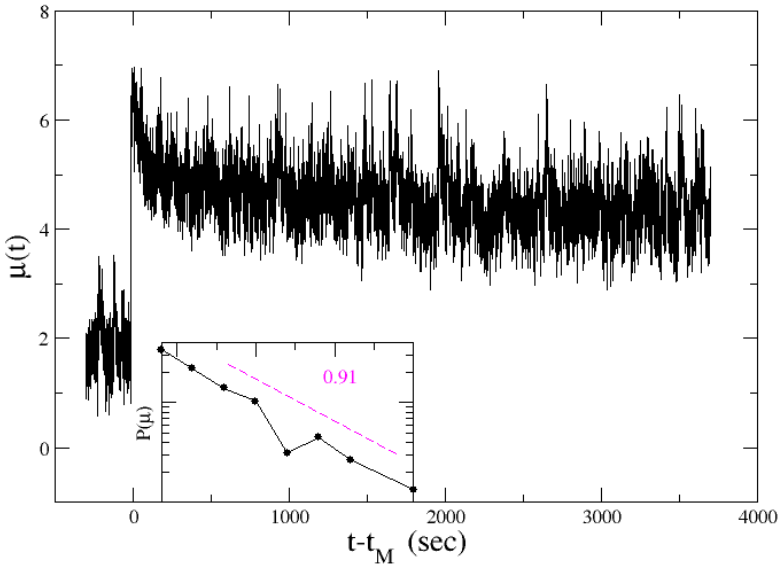

Figure 35: In main panel we plot the envelope function after the Mw6.6 Norcia event. (Inset) Distribution of the percieved magnitude $P(\mu)$ calculated considering all aftershocks with percieved magnitude $\mu = \mu_M - 3$ in a 24-hours time window after the mainshock occurrence.

2.11 KURAYOSHI 2016/10/21

A Mw6.6 earthquake struck Tottori prefecture on 21 October 2016. The event was at relatively shallow depth of 13 km at 6 km S of Kurayoshi, Japan.

Table 18: W-phase Moment Tensor for Kurayoshi

Moment	$2.818E18$ N-m
Magnitude	6.23 Mw
Depth	13.5 km
Half duration	3.00 sec

	Strike	**Dip**	**Rake**
NP1	338°	82°	−19°
NP2	71°	71°	−171°

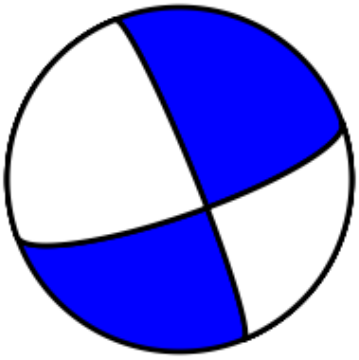

Figure 36: Beach ball for Kurayoshi

The network and the name of the considered seismic station is N.AKSH at coordinates 35.4667N, 133.6307E at altitude 114 m with sampling frequency of 100 Hz.

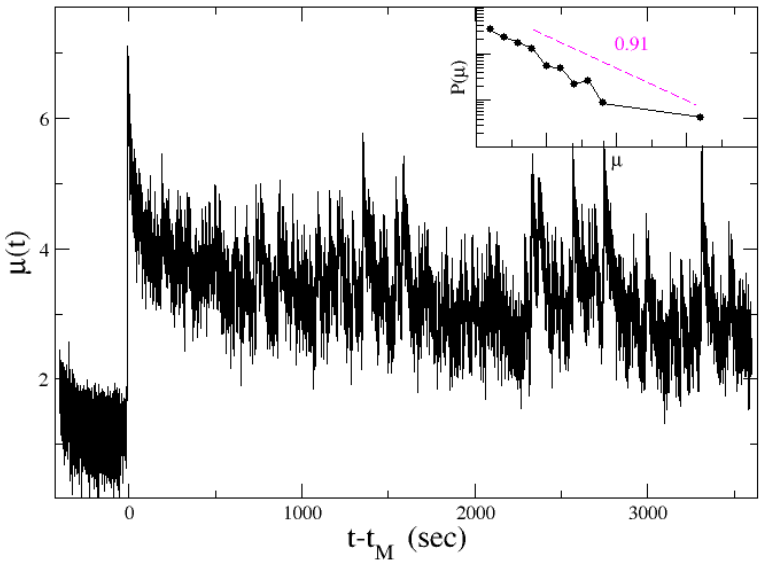

Figure 37: In main panel we plot the envelope function after the Kurayoshi earthquake. (Inset) Distribution of the percieved magnitude $P(\mu)$ calculated considering all aftershocks with percieved magnitude $\mu = \mu_M - 3$ in a 24-hours time window after the mainshock occurrence.

2.12 ISHINOMAKI 2016/11/11

A Mw6.1 earthquake occurred at 24 km ENE of Ishinomaki, Japan. The earthquake was of a depth of about 50 km.

Table 19: W-phase Moment Tensor for Ishinomaki

Moment	$1.937E18$ N-m
Magnitude	6.12 Mw
Depth	50.5 km
Half duration	9.00 sec

	Strike	**Dip**	**Rake**
NP1	202°	20°	95°
NP2	16°	70°	88°

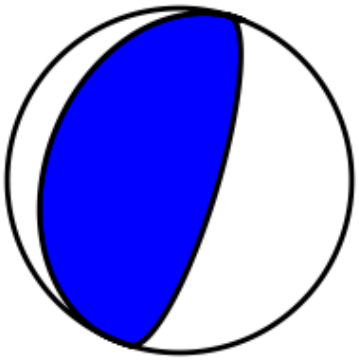

Figure 38: Beach ball for Ishinomaki

The network and the name of the considered seismic station is N.KAKH at coordinates 38.5158N, 141.3421E at altitude 5 m with sampling frequency of 100 Hz.

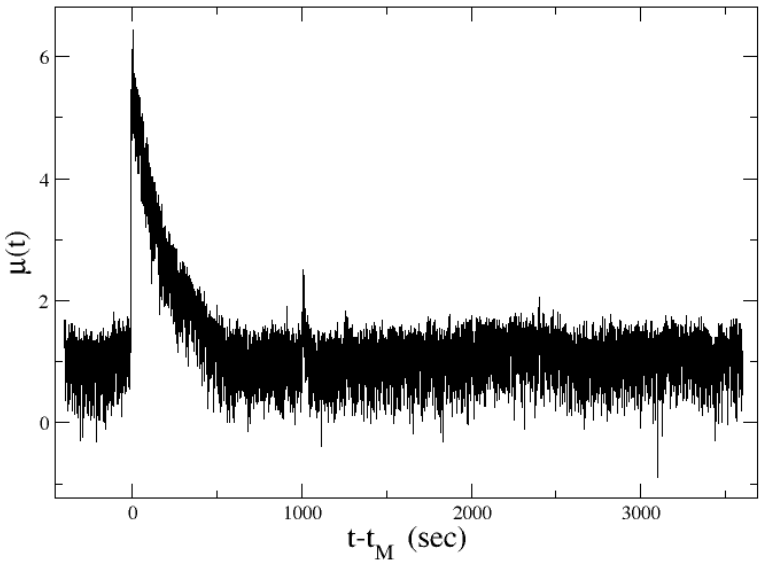

Figure 39: In main panel we plot the envelope function after the Ishinomaki earthquake. We do not plot the distribution of the percieved magnitude $P(\mu)$ because we find only a small number of aftershocks with percieved magnitude $\mu = \mu_M - 3$ in a 24-hours time window after the mainshock occurrence

2.13 NAMIE 2016/11/21

A Mw6.9 earthquake struck 35 km ESE of Namie, Japan. The event occurred if a depth of about 11 km.

Table 20: W-phase Moment Tensor for Namie 2016

Moment	$2.484E19$ N-m
Magnitude	6.86 Mw
Depth	11.5 km
Half duration	7.30 sec

	Strike	**Dip**	**Rake**
NP1	238°	42°	−78°
NP2	42°	49°	−101°

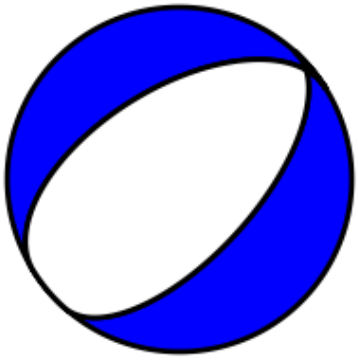

Figure 40: Beach ball for Namie

The network and the name of the considered seismic station is N.HROF at coordinates 37.2246N, 140.8777E at altitude 615 m with sampling frequency of 100 Hz.

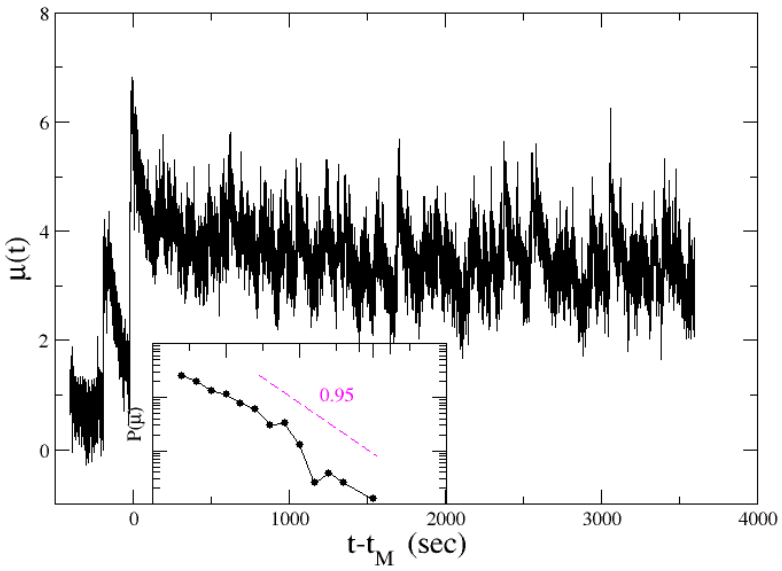

Figure 41: In main panel we plot the envelope function after the Namie earthquake. (Inset) Distribution of the percieved magnitude $P(\mu)$ calculated considering all aftershocks with percieved magnitude $\mu = \mu_M - 3$ in a 24-hours time window after the mainshock occurrence.

2.14 FERNDALE 2016/12/08

A Mw6.6 earthquake struck 164 km W of Ferndale, California. The event occurred as a primarily strike-slip event in the seismically active zone at the boundaty between the Gorda and Pacific plates off the coast of California. The earthquake occurred of a depth of about 11 km.

Table 21: W-phase Moment Tensor for Ferndale

Moment	$1.107E19$ N-m
Magnitude	6.63 Mw
Depth	11.5 km
Half duration	14.00 sec

	Strike	**Dip**	**Rake**
NP1	95°	81°	−159°
NP2	2°	69°	−9°

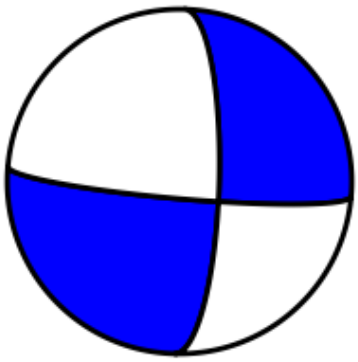

Figure 42: Beach ball for Ferndale

The network and the name of the considered seismic station is NC.KCT at coordinates 40.4755N, 124.3374 O at altitude 378 m with sampling frequency of 100 Hz.

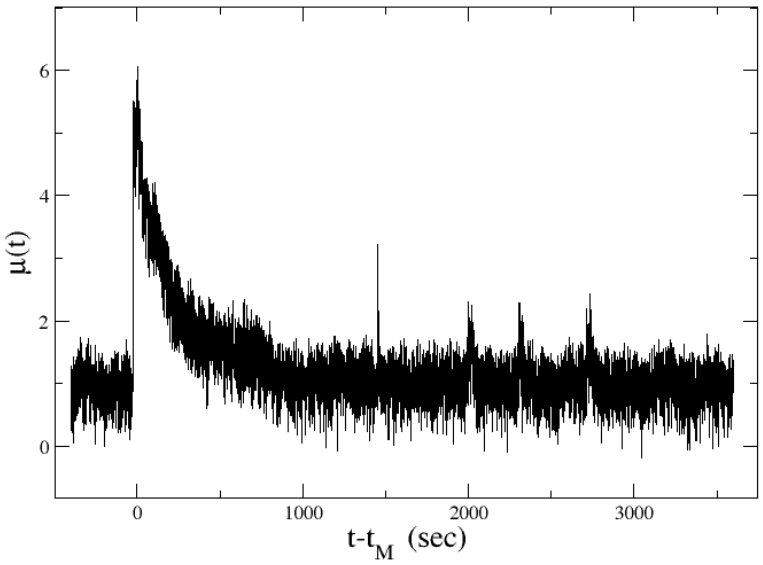

Figure 43: In main panel we plot the envelope function after the Ferndale earthquake. We do not plot the distribution of the percieved magnitude $P(\mu)$ because we find only a small number of aftershocks with percieved magnitude $\mu = \mu_M - 3$ in a 24-hours time window after the mainshock occurrence

2.15 VALPARAISO 2017/04/23 - 2017/04/24

The 2017 sequence occurred in a region where positive loading (increase in the Couloms stress between 0.04 and 0.1 Mpa) was observed. This confirms that the 2017 sequence is located in a seismic gap of the previous large events confined to a small area in a region of low slip between the two major asperities of the 1985 M8.0 Valparaso earthquake. Foreshocks and aftershocks of the 2017 M6.9 event surround the main slip patch of this large earthquake.

REFERENCES

Nealy, J. L., M. W. Herman, G. L. Moore, G. P. Hayes, H. M. Benz, E. A. Bergman, and S. E. Barrientos (2017), 2017 Valparaso earthquake sequence and the megathrust patchwork of central Chile, Geophys. Res. Lett., 44, 88658872, doi:10.1002/2017GL074767.

Table 22: W-phase Moment Tensor for Valparaiso foreshock

Moment	$1.132E18$ N-m
Magnitude	5.97 Mw
Depth	23.5 km
Half duration	2.65 sec

	Strike	**Dip**	**Rake**
NP1	184°	74°	91°
NP2	2°	16°	88°

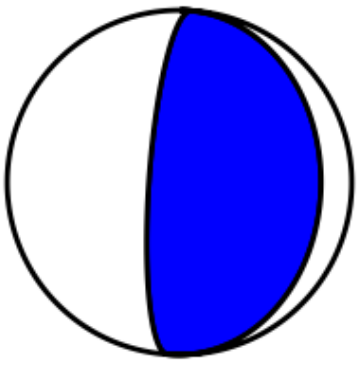

Figure 44: Beach ball for Valparaiso 1

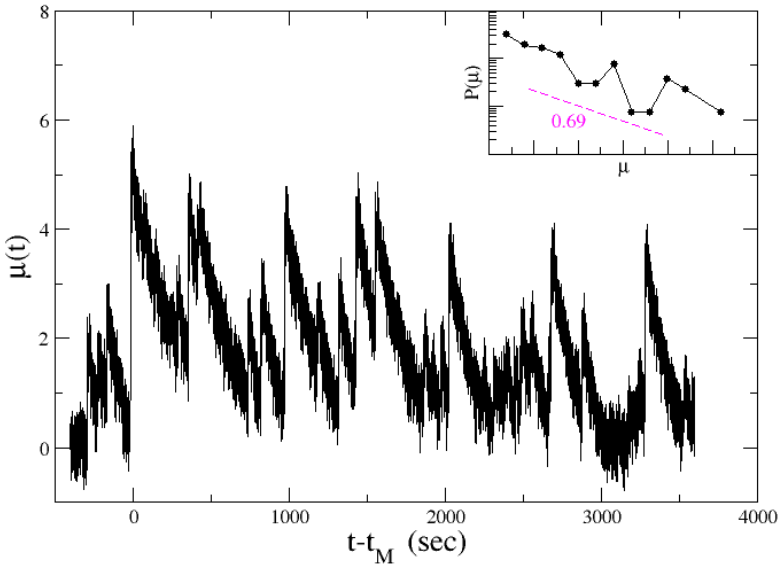

Figure 45: In main panel we plot the envelope function after the Mw6.0 Valparaiso foreshock. (Inset) Distribution of the percieved magnitude $P(\mu)$ calculated considering all aftershocks with percieved magnitude $\mu = \mu_M - 3$ in a 24-hours time window after the mainshock occurrence.

Table 23: W-phase Moment Tensor for Valparaiso mainshock

Moment	$2.775E19$ N-m
Magnitude	6.90 Mw
Depth	25.5 km
Half duration	15.00 sec

	Strike	**Dip**	**Rake**
NP1	4°	14°	99°
NP2	174°	76°	88°

The network and the name of the considered seismic station is C1.MT02 at coordinates 33.2591N, 71.1377 O at altitude 323 m with sampling frequency of 100 Hz.

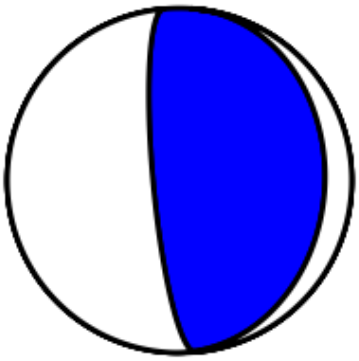

Figure 46: Beach ball for Valparaiso mainshock

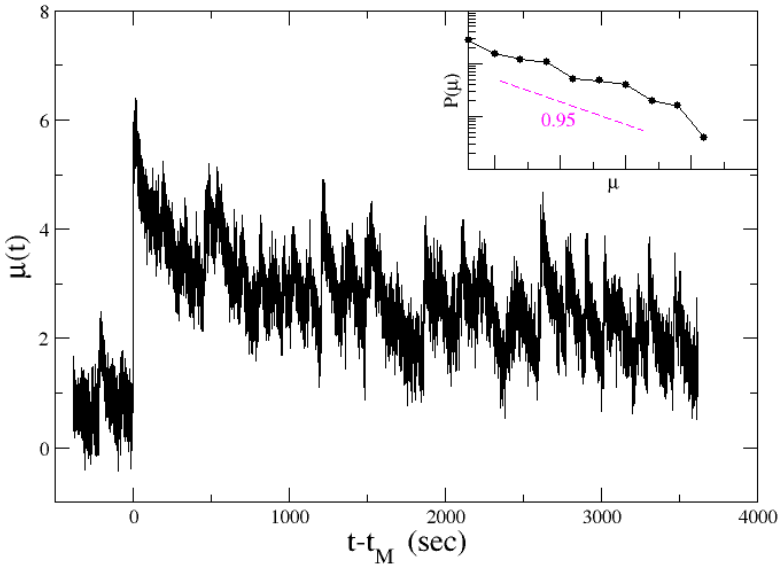

Figure 47: In main panel we plot the envelope function after the Mw6.9 Valparaiso mainshock. (Inset) Distribution of the percieved magnitude $P(\mu)$ calculated considering all aftershocks with percieved magnitude $\mu = \mu_M - 3$ in a 24-hours time window after the mainshock occurrence.

2.16 LESVOS 2017/07/12

The 12 June 2017 sequence in Lesvos was activated by with the occurrence of the Mw6.4 mainshock. The activity gradually migrated NW of the big event and then SE. A strong subsequent was generated by the largest Mw5.2 aftershock if 17 June; after that, the activity slowly decreased. A complex stress field is inferred south of Lesvos, capable of producing E-W strike-slip fauting. A similar pattern is inferred in the north Aegean region. The distribution of stress explains well the presence of aftershocks to the western part of the area, whereas the strike slip kinematics better explains the largest Mw5.2 aftershock.

REFERENCES

P. Papadimitriou, I. Kassaras, G. Kaviris, G.-A. Tselentis, N. Voulgaris, E. Lekkas, G. Chouliaras, C. Evangelidis, K. Pavlou, V. Kapetanidis, A. Karakonstantis, D. Kazantzidou-Firtinidou, I. Fountoulakis, C. Millas, I. Spingos, T. Aspiotis, A. Moumoulidou, E. Skourtsos, V. Antoniou, E. Andreadakis, S. Mavroulis, M. Kleanthi, The 12th June 2017 Mw = 6.3 Lesvos earthquake from detailed seismological observations, Journal of Geodynamics, Volume 115, 2018, Pages$23-42$, ISSN $0264-3707$, https://doi.org/10.1016/j.jog.2018.01.009.

Table 24: W-phase Moment Tensor for Lesvos

Moment	$3.980E18$ N-m
Magnitude	6.33 Mw
Depth	11.5 km
Half duration	3.68 sec

	Strike	**Dip**	**Rake**
NP1	$279°$	$33°$	$-102°$
NP2	$114°$	$57°$	$-82°$

The network and the name of the considered seismic station is HL.PRK at coordinates 39.2456N, 26.2649E at altitude 130 m with sampling frequency of 100 Hz.

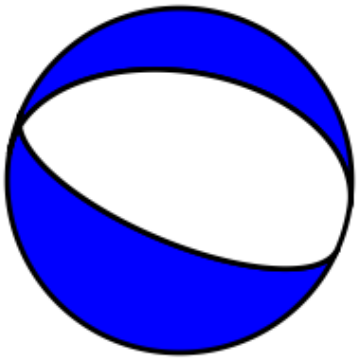

Figure 48: Beach ball for Lesvos

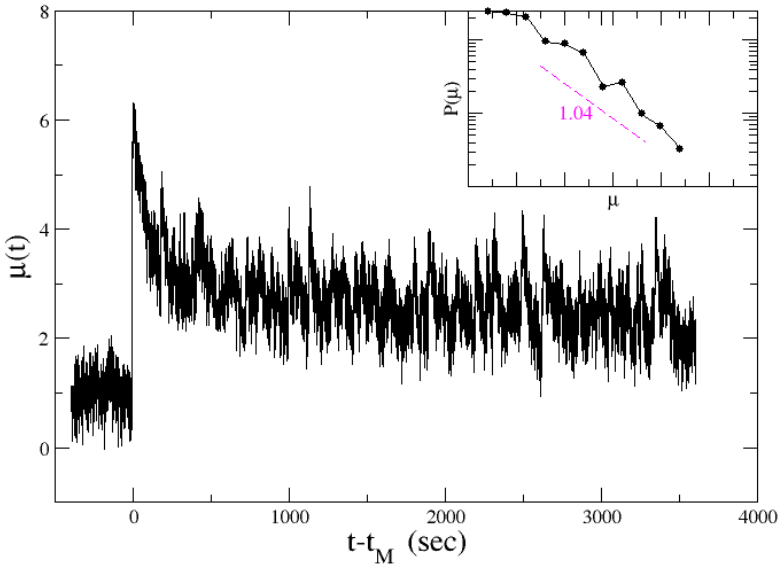

Figure 49: In main panel we plot the envelope function after the Lesvos earthquake. (Inset) Distribution of the percieved magnitude $P(\mu)$ calculated considering all aftershocks with percieved magnitude $\mu = \mu_M - 3$ in a 24-hours time window after the mainshock occurrence.

2.17 KOS 2017/07/20

The 20 July 2017 was characterized of a Mw6.6 destructive earthquake associated with a small tsunami. At the beginning there was an abinguity of fault dip direction but, the results of (Konca et. al) study strongly support a north-dipping coseismic fault. The early aftershocks activity propagates in every direction and significant activity can be observed toward east and west direction. Even for the Coulomb stress change, at the beginning there was abinguity because the variation of the slip distributions generate different Coulomb stress perturbation in depth. However the results shows that in the range of significant slip (4-10 km) the north-dipping model is more consistent with the seismicity.

REFERENCES A. O. Konca, S. E. Guvercin, S. Ozarpaci, A. Ozdemir, G. J. Funning, U. Dogan, S. Ergintav, M. Floyd, H. Karabulut, R. Reilinger, Slip distribution of the 2017 Mw6.6 BodrumKos earthquake: resolving the ambiguity of fault geometry, Geophysical Journal International, Volume 219, Issue 2, November 2019, Pages 911923, https://doi.org/10.1093/gji/ggz332

Table 25: W-phase Moment Tensor for Kos

Moment	$1.105E19$ N-m
Magnitude	6.63 Mw
Depth	11.5 km
Half duration	5.38 sec

	Strike	**Dip**	**Rake**
NP1	$84°$	$53°$	$-103°$
NP2	$285°$	$39°$	$-73°$

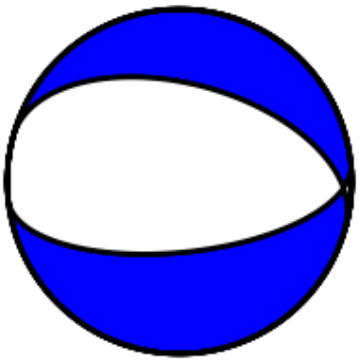

Figure 50: Beach ball for Kos

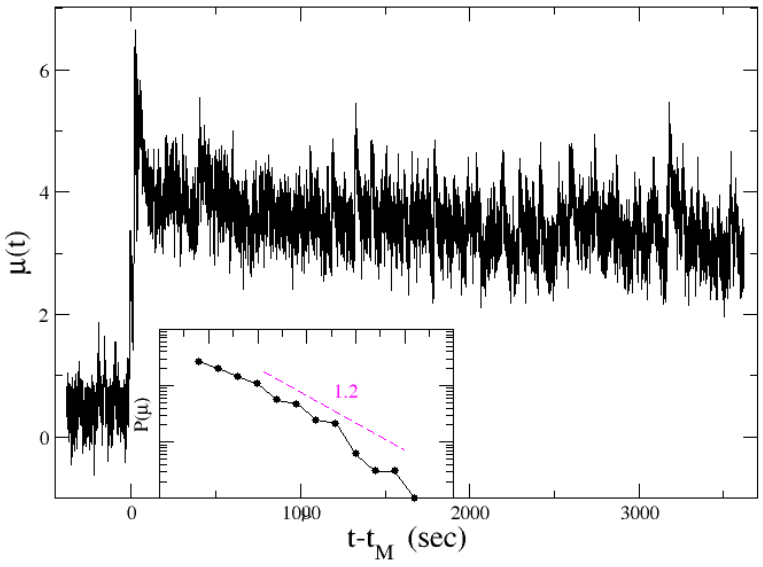

Figure 51: In main panel we plot the envelope function after the Kos earthquake. (Inset) Distribution of the percieved magnitude $P(\mu)$ calculated considering all aftershocks with percieved magnitude $\mu = \mu_M - 3$ in a 24-hours time window after the mainshock occurrence.

The network and the name of the considered seismic station is KO.DAT at coordinates 36.7308N, 27.5767E at altitude 1100 m with sampling frequency of 50 Hz.

2.18 NAZE 2017/07/26

On 26 July 2017 a Mw6.0 earthquake struck 176 km SSE of Naze, Japan. The event occurred at a depth of about 15 km.

Table 26: W-phase Moment Tensor for Naze

Moment	$1.173E18$ N-m
Magnitude	5.98 Mw
Depth	15.5 km
Half duration	2.41 sec

	Strike	**Dip**	**Rake**
NP1	33°	57°	−90°
NP2	213°	33°	−90°

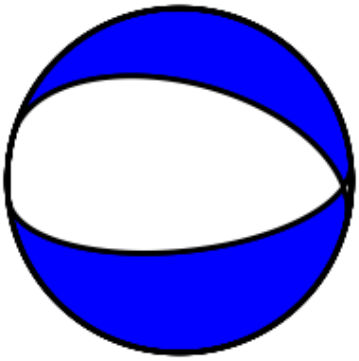

Figure 52: Beach ball for Naze 2017

The network and the name of the considered seismic station is N.KGMF at coordinates 26.7567N, 128.2153E at altitude 102 m with sampling frequency of 100 Hz.

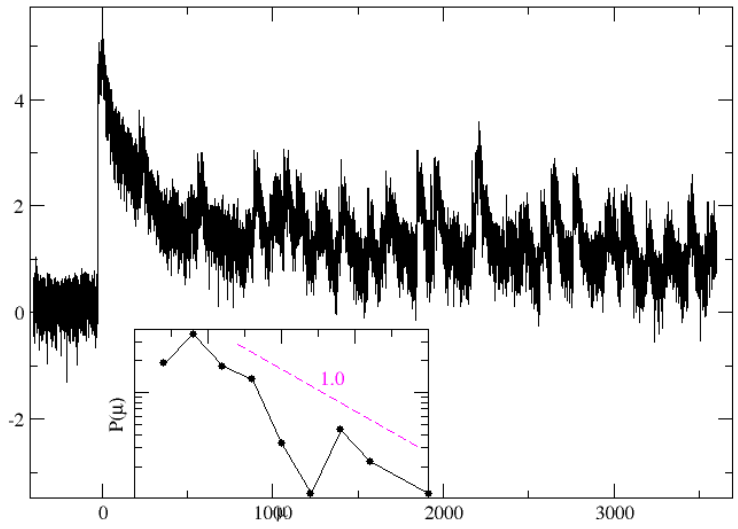

Figure 53: In main panel we plot the envelope function after the Naze earthquake. (Inset) Distribution of the percieved magnitude $P(\mu)$ calculated considering all aftershocks with percieved magnitude $\mu = \mu_M - 3$ in a 24-hours time window after the mainshock occurrence.

2.19 MISAWA 2018/01/24

On 24 January 2018 a Mw6.3 earthquake struck 101 km ENE of Misawa, Japan. The event occurred at a depth of about 50 km.

Table 27: W-phase Moment Tensor for Misawa

Moment	$3.539E18$ N-m
Magnitude	6.30 Mw
Depth	50.5 km
Half duration	3.78 sec

	Strike	**Dip**	**Rake**
NP1	167°	27°	49°
NP2	31°	70°	108°

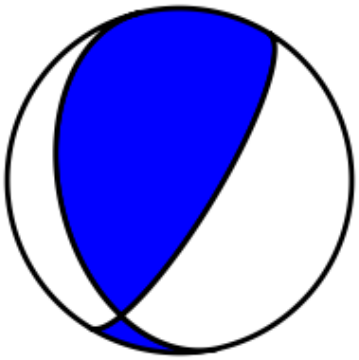

Figure 54: Beach ball for Misawa

The network and the name of the considered seismic station is N.KJNH at coordinates 40.2686N, 141.7831E at altitude 175 m with sampling frequency of 100 Hz.

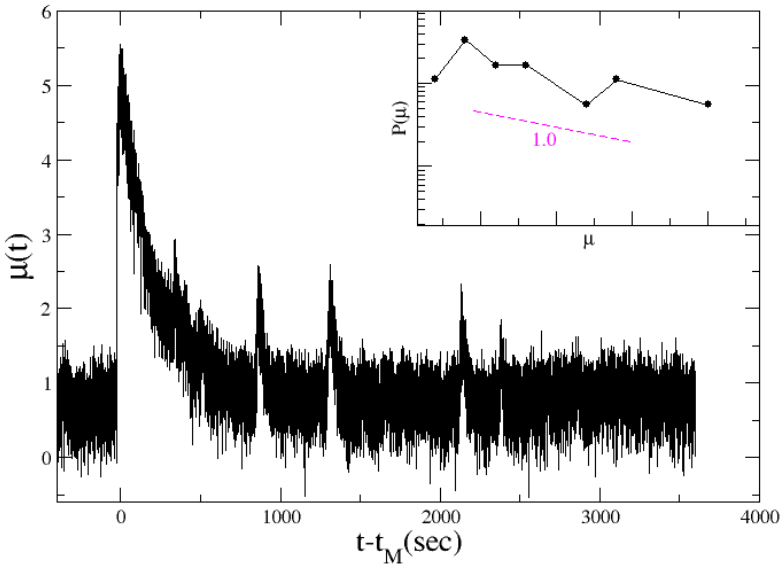

Figure 55: In main panel we plot the envelope function after the Misawa earthquake. (Inset) Distribution of the percieved magnitude $P(\mu)$ calculated considering all aftershocks with percieved magnitude $\mu = \mu_M - 3$ in a 24-hours time window after the mainshock occurrence.

2.20 HUALIEN 2018/02/04 - 2018/02/06

Mw6.4 earthquake hit Hualien on 6 February 2018 and was anticipated by a Mw6.2 event occurred in the offshore area of Hualien City in 4 February 2018. The latter was followed by more than 50 events of local magnitude $Mw3+$ and is characterized with a low b-value. Regarding the Mw6.4 event, focal mechanism and aftershock distribution both suggested a west-dipping fault plane. However, based on the geological investigation (Chen 2018), the surface ruptures were observed along the east-dipping Milun fault trace and the aftershocks occurred on the southern part also indicated an east-dipping fault plane.

REFERENCES

Wen, Y.-Y., S. Wen, Y.-H. Lee, and K.-E. Ching, 2019: The kinematic source analysis for 2018 Mw 6.4 Hualien, Taiwan earthquake. Terr. Atmos. Ocean. Sci., 30, 377-387, doi:10.3319/TAO.2018.11.15.03

Chen, P.-F., Y.-L. Chen, P.-L. Su, Y.-D. Peng, and L.-F. Chen, 2019: Understanding the 6 February 2018, Hualien earthquake sequence through catalog compilation. Terr. Atmos. Ocean. Sci., 30, 399-409, doi: 10.3319/TAO.2018.11.15.02

Table 28: W-phase Moment Tensor for Hualien foreshock

Moment	$1.826E18$ N-m
Magnitude	6.11 Mw
Depth	15.5 km
Half duration	2.76 sec

	Strike	**Dip**	**Rake**
NP1	298°	14°	138°
NP2	70°	81°	80°

Table 29: W-phase Moment Tensor for Hualien 2

Moment	$5.349E18$ N-m
Magnitude	6.42 Mw
Depth	19.5 km
Half duration	3.93 sec

	Strike	**Dip**	**Rake**
NP1	209°	73°	22°
NP2	112°	69°	161°

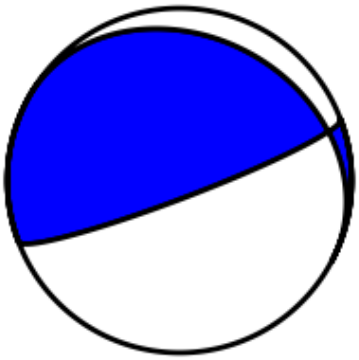

Figure 56: Beach ball for Hualien 1

The network and the name of the considered seismic station is TW.CHGB at coordinates 24.0602N, 121.1740E at altitude 1850 m with sampling frequency of 20 Hz.

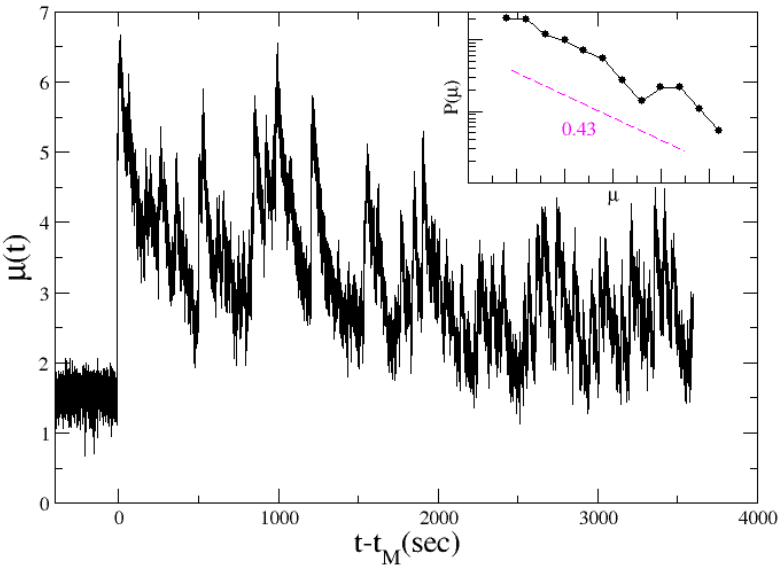

Figure 57: In main panel we plot the envelope function after the Mw6.2 Hualien foreshock. (Inset) Distribution of the percieved magnitude $P(\mu)$ calculated considering all aftershocks with percieved magnitude $\mu = \mu_M - 3$ in a 24-hours time window after the mainshock occurrence.

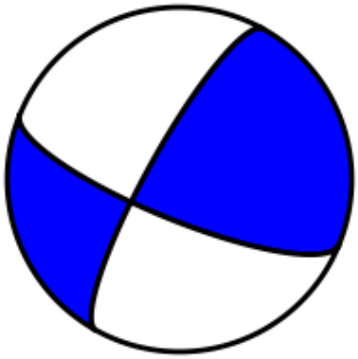

Figure 58: Beach ball for Hualien 2

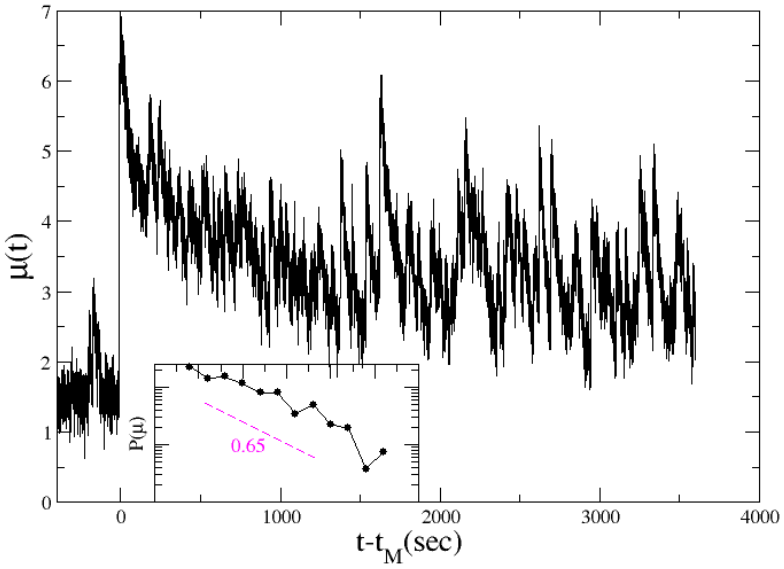

Figure 59: In main panel we plot the envelope function after the Mw6.4 Hualien mainshock. (Inset) Distribution of the percieved magnitude $P(\mu)$ calculated considering all aftershocks with percieved magnitude $\mu = \mu_M - 3$ in a 24-hours time window after the mainshock occurrence.

2.21 OREGON 2018/08/22

A Mw6.2 earthquake struck 272 km WNW of Bandon, Oregon. The event occurred of a depth of about 15 km.

Table 30: W-phase Moment Tensor for Oregon 2018

Moment	$2.131E18$ N-m
Magnitude	6.15 Mw
Depth	15.5 km
Half duration	3.04 sec

	Strike	**Dip**	**Rake**
NP1	115°	89°	−165°
NP2	24°	75°	−1°

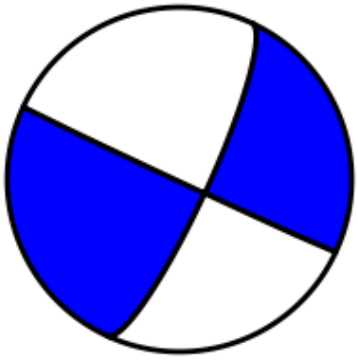

Figure 60: Beach ball for Oregon 2018

The network and the name of the considered seismic station is NC.KEB at coordinates 42.8722N, 124.3342 O at altitude 818 m with sampling frequency of 100 Hz.

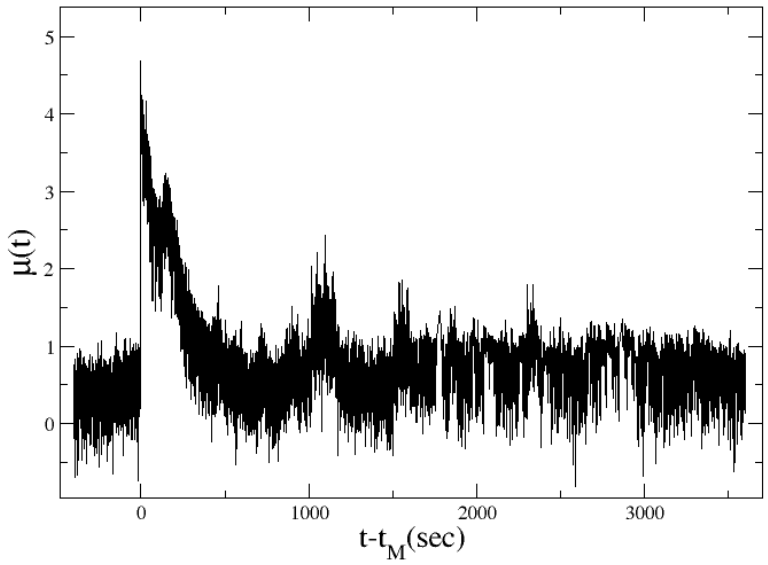

Figure 61: In main panel we plot the envelope function after the Oregon earthquake. We do not plot the distribution of the percieved magnitude $P(\mu)$ because we find only a small number of aftershocks with percieved magnitude $\mu = \mu_M - 3$ in a 24-hours time window after the mainshock occurrence

2.22 TOMAKOMAI 2018/09/05

A Mw6.7 earthquake hit northern Japan near the major city of Sapporo. The quake epicenter was about 27.3 km east of the city of Tomakomai. The event occurred of a depth of about 40 km.

Table 31: W-phase Moment Tensor for Tomakomai

Moment	$1.016E19$ N-m
Magnitude	6.60 Mw
Depth	40.5 km
Half duration	4.96 sec

	Strike	**Dip**	**Rake**
NP1	333°	61°	83°
NP2	167°	30°	102°

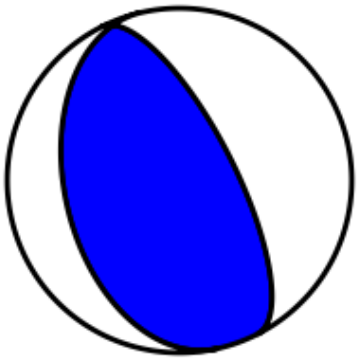

Figure 62: Beach ball for Tomakomai

The network and the name of the considered seismic station is N.BRWH at coordinates 42.7031N, 142.2296E at altitude 82 m with sampling frequency of 100 Hz.

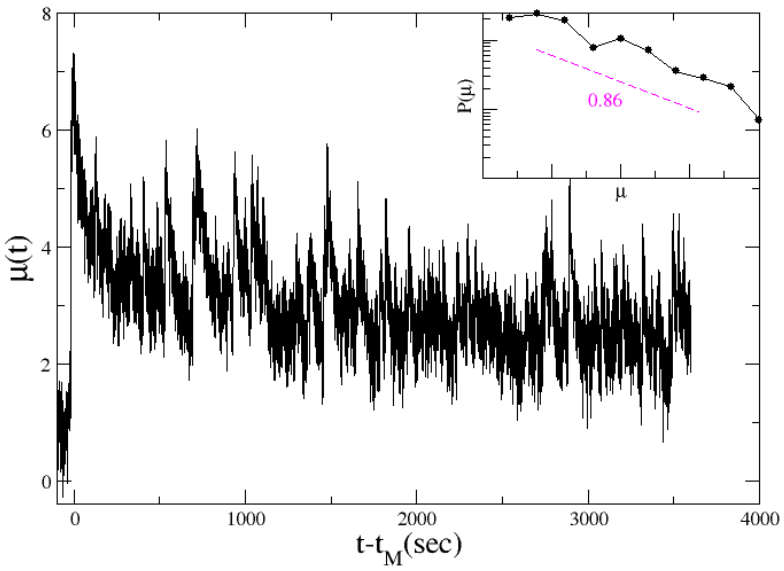

Figure 63: In main panel we plot the envelope function after the Tomakomai earthquake. (Inset) Distribution of the percieved magnitude $P(\mu)$ calculated considering all aftershocks with percieved magnitude $\mu = \mu_M - 3$ in a 24-hours time window after the mainshock occurrence.

2.23 PORT HARDY 2018/10/22

Two major earthquakes occurred within 37 minutes of one another off west coast of Vancouver Island. The first, a Mw6.5, struck at 05:39 UTC on 2018-10-22. It was 218 km southwest of Port Hardy at a depth of about 20 km. The second (Mw6.8) happened at 06:16 on 2018-10-22only 37 minutes later after the first foreshock. It was 232 km southwest of Port Hardy at a depth of about 21 km.

Table 32: W-phase Moment Tensor for Port Hardy 2018 foreshock

Moment	$8.082E18$ N-m
Magnitude	6.54 Mw
Depth	21.5 km
Half duration	5.49 sec

	Strike	**Dip**	**Rake**
NP1	307°	86°	169°
NP2	38°	79°	4°

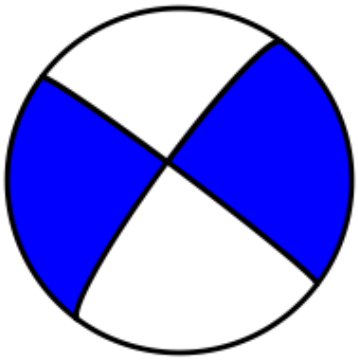

Figure 64: Beach ball for Port Hardy 1

Table 33: W-phase Moment Tensor for Port Hardy mainshock

Moment	$1.880E19$ N-m
Magnitude	6.78 Mw
Depth	21.5 km
Half duration	6.78 sec

	Strike	**Dip**	**Rake**
NP1	309°	80°	−174°
NP2	218°	84°	−10°

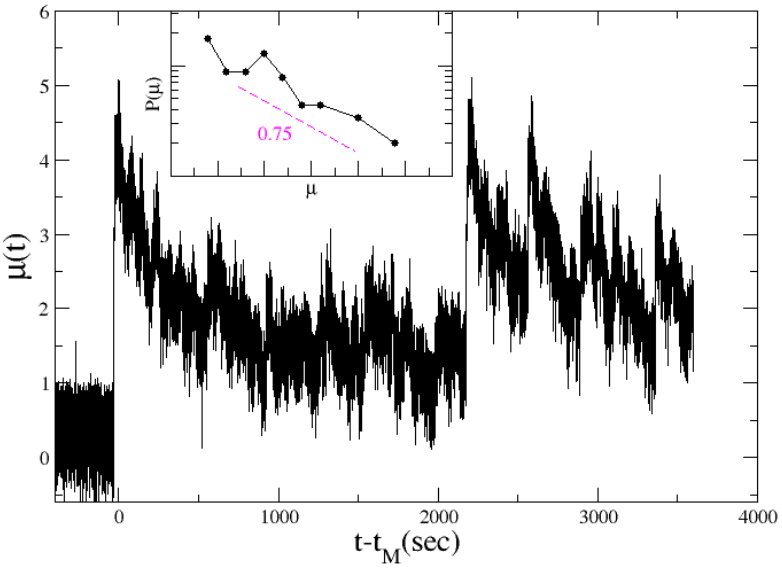

Figure 65: In main panel we plot the envelope function after the Mw6.5 Port Hardy earthquake. (Inset) Distribution of the percieved magnitude $P(\mu)$ calculated considering all aftershocks with percieved magnitude $\mu = \mu_M - 3$ in a 24-hours time window after the mainshock occurrence.

The network and the name of the considered seismic station is CN.PBEB at coordinates 50.1566N, 127.7719 O at altitude 732 m with sampling frequency of 100 Hz.

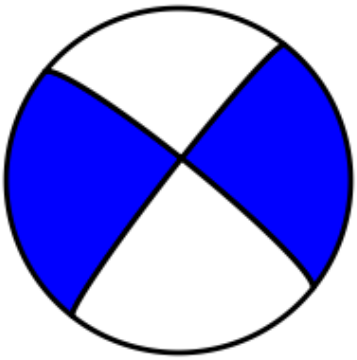

Figure 66: Beach ball for Port Hardy mainshock

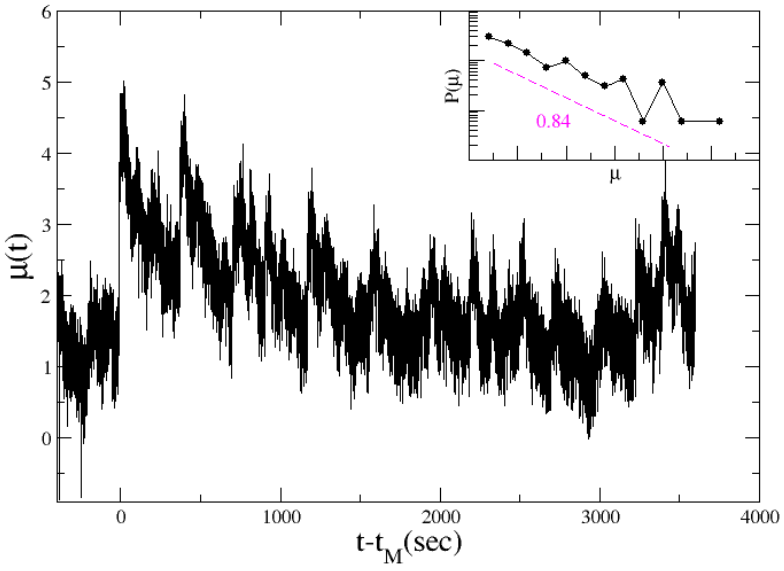

Figure 67: In main panel we plot the envelope function after the Mw6.8 Port Hardy second earthquake. (Inset) Distribution of the percieved magnitude $P(\mu)$ calculated considering all aftershocks with percieved magnitude $\mu = \mu_M - 3$ in a 24-hours time window after the mainshock occurrence.

2.24 ZAKYNTHOS 2018/10/25

A Mw6.8 earthquake occurred 45 km southwest of Zakynthos. The event was followed by a standard exponetially decaying aftershock sequence which included one Mw5.1 event immediately after mainshock, and four other events of Mw5+ in the first week. The general activity in the first day after the mainshock, occupied an area of $\sim 20\times20$ km; while in the next days, a much broaded area was activated. The slip inversion is not easy because the epicentral distances are relatively large and the azimuthal coverage is poor. Nevertheless, the model proposed by (Sokos et al.), consisting of two segments, fits the seismic data better than the single-fault model.

REFERENCES

Sokos, E., F. Gallovi, C. P. Evangelidis, A. Serpetsidaki, V. Plicka, J. Kosteleck, and J. Zahradnk (2020). The 2018 Mw 6.8 Zakynthos, Greece, Earthquake: Dominant Strike-Slip Faulting near Subducting Slab, Seismol. Res. Lett. XX, 112, doi: 10.1785/0220190169.

Table 34: W-phase Moment Tensor for Zakynthos

Moment	$1.714E19$ N-m
Magnitude	6.76 Mw
Depth	19.5 km
Half duration	6.60 sec

	Strike	**Dip**	**Rake**
NP1	9°	39°	167°
NP2	109°	82°	52°

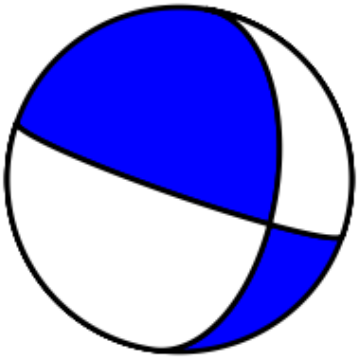

Figure 68: Beach ball for Zakynthos

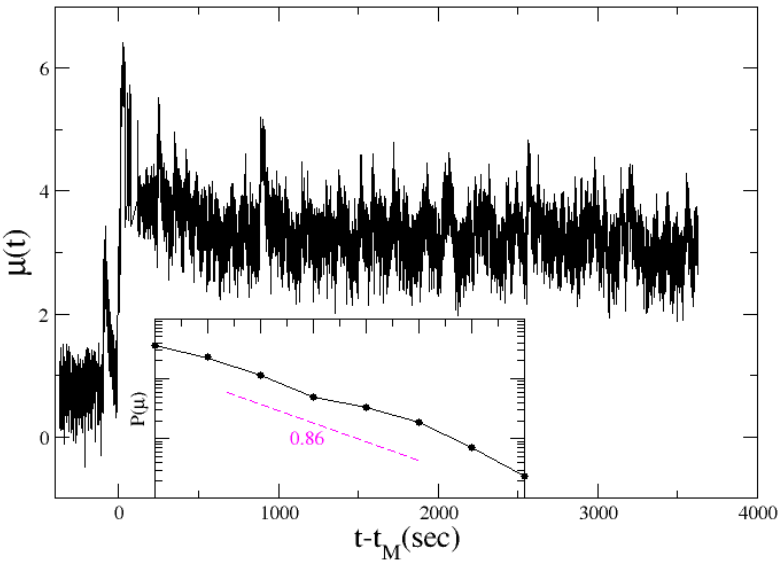

Figure 69: In main panel we plot the envelope function after the Zakynthos earthquake. (Inset) Distribution of the percieved magnitude $P(\mu)$ calculated considering all aftershocks with percieved magnitude $\mu = \mu_M - 3$ in a 24-hours time window after the mainshock occurrence.

The network and the name of the considered seismic station is HT.RTZL at coordinates 38.076N, 20.7715E at altitude 103 m with sampling frequency of 100 Hz.

2.25 NISHINOOMOTE 2019/01/08

On 08 January 2019 a Mw6.3 earthquake struck 16 km SSE of Nishinoomote, Japan. The event occurred at a depth of about 30 km.

Table 35: W-phase Moment Tensor for Nishinoomote

Moment	$3.335E18$ N-m
Magnitude	6.28 Mw
Depth	30.5 km
Half duration	3.62 sec

	Strike	**Dip**	**Rake**
NP1	215°	34°	80°
NP2	47°	57°	96°

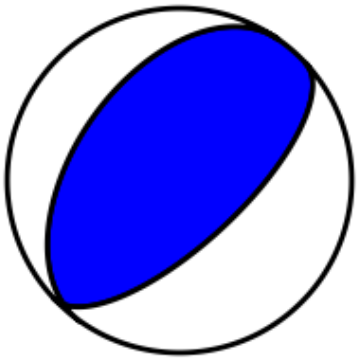

Figure 70: Beach ball for Nishinoomote

The network and the name of the considered seismic station is N.UCNH at coordinates 31.2583N, 131.0877E at altitude 265 m with sampling frequency of 100 Hz.

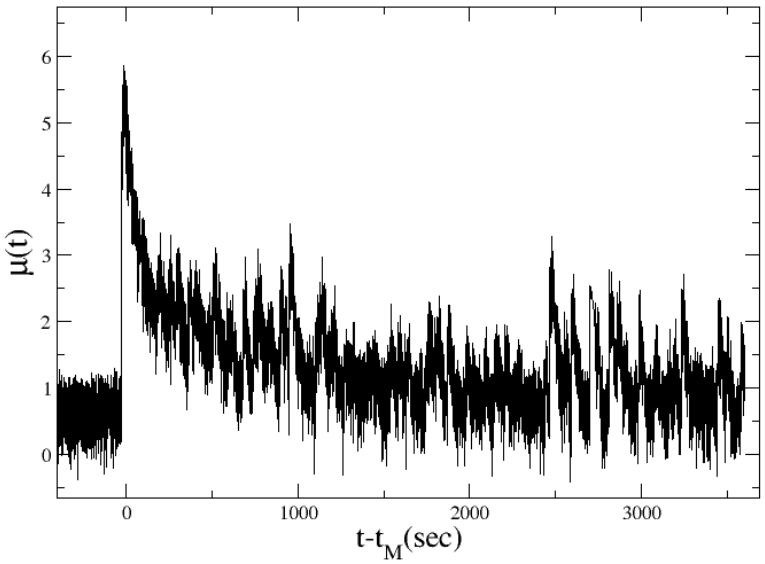

Figure 71: In main panel we plot the envelope function after the Nishinoomote earthquake. We do not plot the distribution of the percieved magnitude $P(\mu)$ because we find only a small number of aftershocks with percieved magnitude $\mu = \mu_M - 3$ in a 24-hours time window after the mainshock occurrence

2.26 TSURUOKA 2019/06/18

An earthquake Mw6.4 struck the Hokuriku region centered in Tsuruoka in Japan on 18 June 2019. The earthquake was about 31 km WSW of Tsuruoka and occurred of a depth of about 19 km.

Table 36: W-phase Moment Tensor for Tsuruoka

Moment	$5.484E18$ N-m
Magnitude	6.43 Mw
Depth	19.5 km
Half duration	4.09 sec

	Strike	**Dip**	**Rake**
NP1	210°	52°	92°
NP2	27°	38°	88°

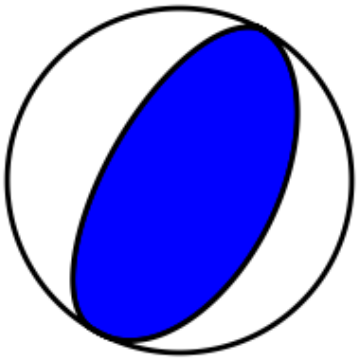

Figure 72: Beach ball for Tsuruoka

The network and the name of the considered seismic station is N.ASAH at coordinates 38.4704N, 139.7606E at altitude 265 m with sampling frequency of 100 Hz.

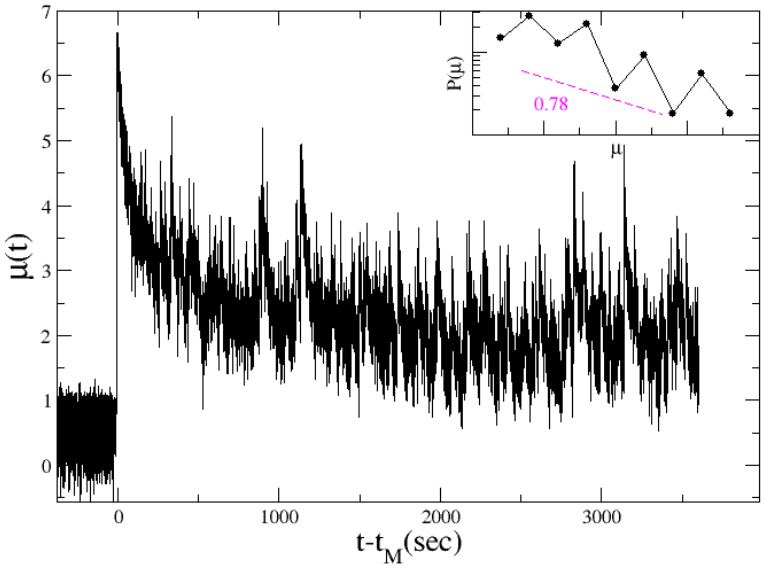

Figure 73: In main panel we plot the envelope function after the Tsuruoka earthquake. (Inset) Distribution of the percieved magnitude $P(\mu)$ calculated considering all aftershocks with percieved magnitude $\mu = \mu_M - 3$ in a 24-hours time window after the mainshock occurrence.

2.27 RIDGECREST 2019/07/04 - 2019/07/06

The Coulomb stress increased of 0.66 bar on the hypocentral patch of the Mw7.1 earthquake due the occurrence of the Mw6.4 foreshock. However the increase is not restricted to the hypocentral area and the surrounding $\sim 5\times 20$km patch of the future rupture was brought > 2 bar closer to failure. Conversely, the southern portion of the Mw7.1 rupture surface was inhibited by > 5 bars; presumably this was overcome by the much larger dynamic stresses shed off the Mw7.1 rupture front as it propagated southward. Just 2.5 km from the hypocenter of the Mw7.1, an Mw5.4 shock struck 17.5 hr after the Mw 6.4, 16.2 hr before the Mw7.1. Although the stress imparted by the Mw5.4 to the Mw7.1 hypocenter is sensitive to its unknown rupture dimensions, location uncertainties, and the strike of the Mw5.4 fault, it was likely at least several bars, or higher than that of the Mw6.4.

REFERENCES

Shinji Toda and Ross S. Stein Long- and Short-Term Stress Interaction of the 2019 Ridgecrest Sequence and Coulomb-Based Earthquake Forecasts Bull. Seismol. Soc. Am. XX, 116, doi: 10.1785/0120200169

Table 37: W-phase Moment Tensor for Ridgecrest foreshock 1

Moment	$4.918E18$ N-m
Magnitude	6.39 Mw
Depth	8.0 km
Half duration	– sec

	Strike	**Dip**	**Rake**
NP1	228°	66°	4°
NP2	137°	86°	156°

Table 38: W-phase Moment Tensor for Ridgecrest mainshock

Moment	$2.712E19$ N-m
Magnitude	6.89 Mw
Depth	8.0 km
Half duration	– sec

	Strike	**Dip**	**Rake**
NP1	322°	81°	−173°
NP2	231°	83°	−9°

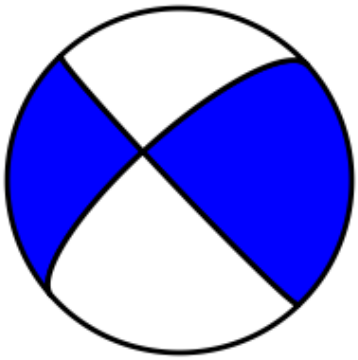

Figure 74: Beach ball for Ridgecrest 1

The network and the name of the considered seismic station is PB.B196 at coordinates 36.1925N, 117.6685 O at altitude 1859 m with sampling frequency of 100 Hz.

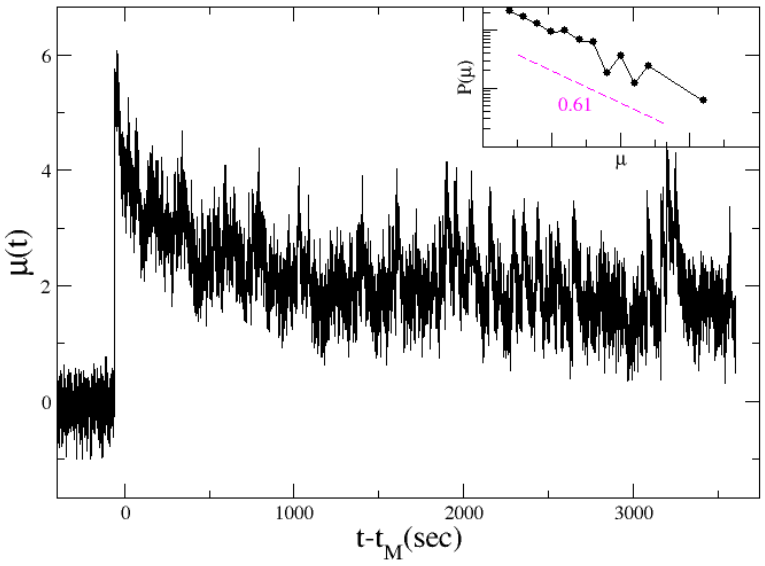

Figure 75: In main panel we plot the envelope function after the Mw6.4 Ridgecrest foreshock. (Inset) Distribution of the percieved magnitude $P(\mu)$ calculated considering all aftershocks with percieved magnitude $\mu = \mu_M - 3$ in a 24-hours time window after the mainshock occurrence.

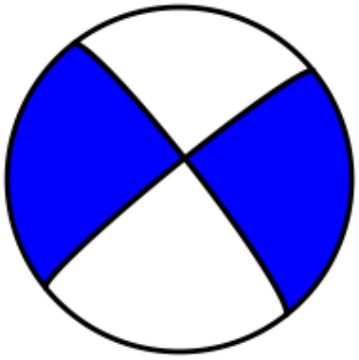

Figure 76: Beach ball for Ridgecrest mainshock

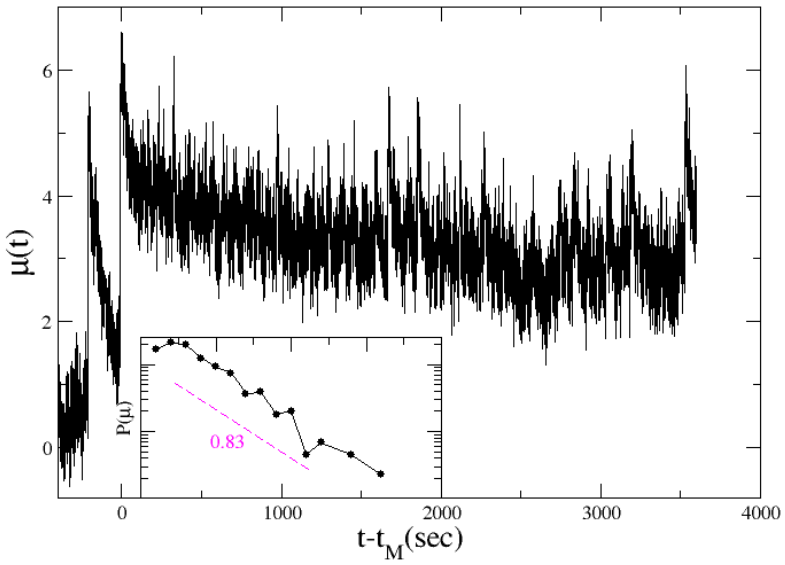

Figure 77: In main panel we plot the envelope function after the Mw7.0 Ridgecrest mainshock. (Inset) Distribution of the percieved magnitude $P(\mu)$ calculated considering all aftershocks with percieved magnitude $\mu = \mu_M - 3$ in a 24-hours time window after the mainshock occurrence.

2.28 BELLA BELLA 2019/07/04

A Mw6.2 earthquake struck 192 km WSW of Bella Bella, Canada. The event occurred of a depth of about 11 km.

Table 39: W-phase Moment Tensor for Bella Bella

Moment	$2.753E18$ N-m
Magnitude	6.23 Mw
Depth	11.5 km
Half duration	3.33 sec

	Strike	**Dip**	**Rake**
NP1	255°	66°	−3°
NP2	346°	88°	−156°

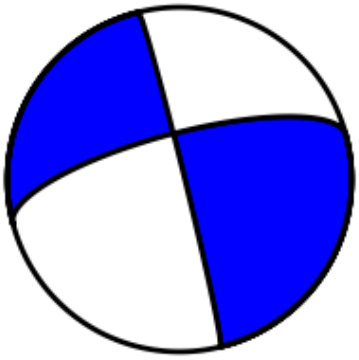

Figure 78: Beach ball for Bella Bella

The network and the name of the considered seismic station is CN.BBB at coordinates 52.1847N, 128.1133 O at altitude 14 m with sampling frequency of 40 Hz.

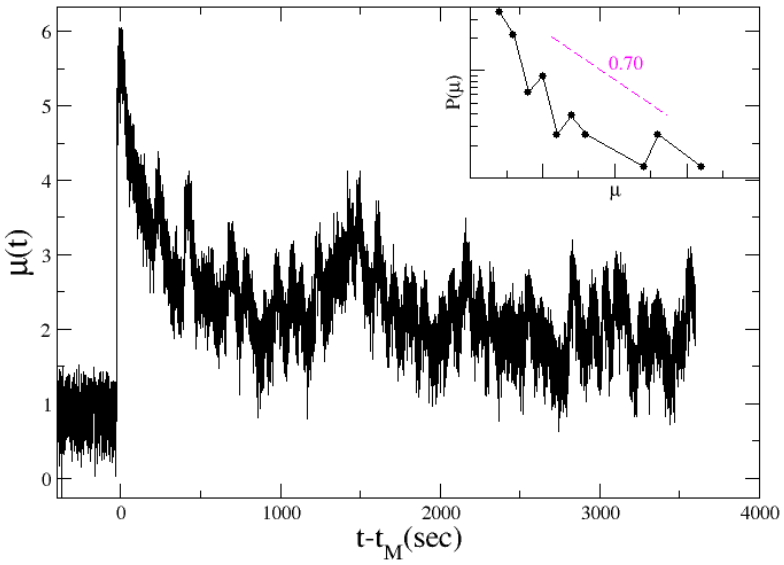

Figure 79: In main panel we plot the envelope function after the Bella Bella earthquake. (Inset) Distribution of the percieved magnitude $P(\mu)$ calculated considering all aftershocks with percieved magnitude $\mu = \mu_M - 3$ in a 24-hours time window after the mainshock occurrence.

2.29 NAMIE 2019/08/04

A Mw6.3 earthquake struck in the Pacific off Fukushima, northeastern Japan. Its epicenter is located 54 km east of Namie, eastern Fukushima. The event occurred of a depth of 20 km.

Table 40: W-phase Moment Tensor for Namie 2019

Moment	$3.321E18$ N-m
Magnitude	6.28 Mw
Depth	40.5 km
Half duration	3.28 sec

	Strike	**Dip**	**Rake**
NP1	179°	25°	66°
NP2	26°	67°	101°

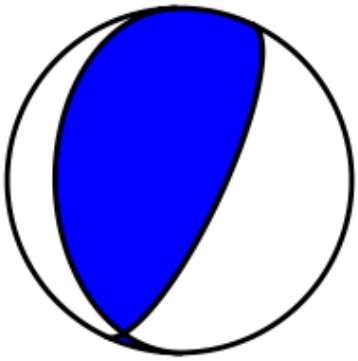

Figure 80: Beach ball for Namie 2019

The network and the name of the considered seismic station is N.RIFH at coordinates 38.3400N, 140.9551E at altitude 48 m with sampling frequency of 100 Hz.

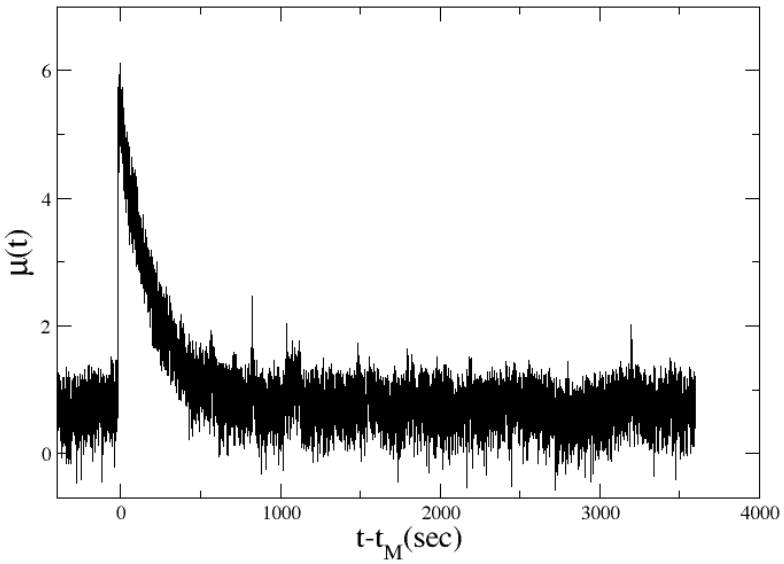

Figure 81: In main panel we plot the envelope function after the Namie 2019 earthquake. We do not plot the distribution of the percieved magnitude $P(\mu)$ because we find only a small number of aftershocks with percieved magnitude $\mu = \mu_M - 3$ in a 24-hours time window after the mainshock occurrence

2.30 OREGON 2019/08/29

A Mw6.3 earthquake struck 285 km W of Bandon, Oregon. The event occurred of a depth of about 11 km.

Table 41: W-phase Moment Tensor for Oregon 2019

Moment	$3.099E18$ N-m
Magnitude	6.26 Mw
Depth	11.5 km
Half duration	3.50 sec

	Strike	**Dip**	**Rake**
NP1	$114°$	$86°$	$-173°$
NP2	$23°$	$83°$	$-4°$

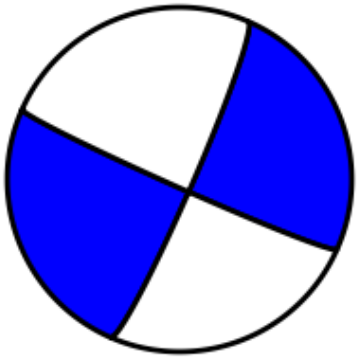

Figure 82: Beach ball for Oregon 2019

The network and the name of the considered seismic station is NC.KEB at coordinates 42.8722N, 124.3342 O at altitude 818 m with sampling frequency of 100 Hz.

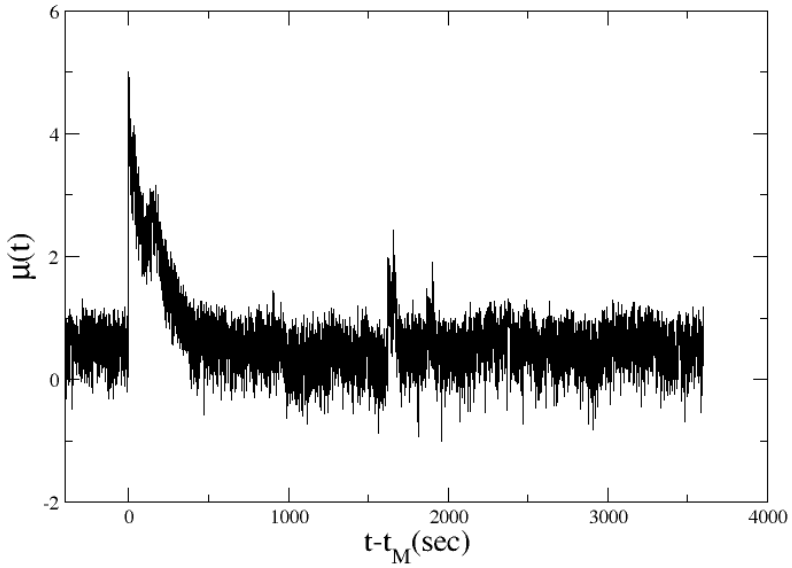

Figure 83: In main panel we plot the envelope function after the Oregon 2019 earthquake. We do not plot the distribution of the percieved magnitude $P(\mu)$ because we find only a small number of aftershocks with percieved magnitude $\mu = \mu_M - 3$ in a 24-hours time window after the mainshock occurrence

2.31 ALBANIA 2019/11/26

Northwestern Albania was struck by a strong Mw6.4 earthquake with an epicentre 16 kilometres (9.9 mi) west-southwest of Mamurras, on 26 November 2019. The tectonics of western and northen Albania are characterized by on-going compression due to collision between the Eurasian plate and the Adriatic block. The western region of Albania has been historically sibject to strong earthquakes. The tectonic zone has a longitudinal extension of SE-NW direction and a dip angle toward the NE direction. The focal mechanism of aftershocks indicate back thrust faulting.

REFERENCES

Ganas, Athanassios, Elias, Panagiotis, Briole, Pierre, Cannav, Flavio, Valkaniotis, Sotirios, Tsironi, Varvara, Partheniou, Eleni. (2020). Ground Deformation and Seismic Fault Model of the M6.4 Durres (Albania) Nov. 26, 2019 Earthquake, Based on GNSS/INSAR Observations. Geosciences. 10. 210. 10.3390/geosciences10060210.

Table 42: W-phase Moment Tensor for Albania

Moment	$4.561E18$ N-m
Magnitude	6.37 Mw
Depth	19.5 km
Half duration	3.89 sec

	Strike	**Dip**	**Rake**
NP1	338°	27°	92°
NP2	156°	63°	89°

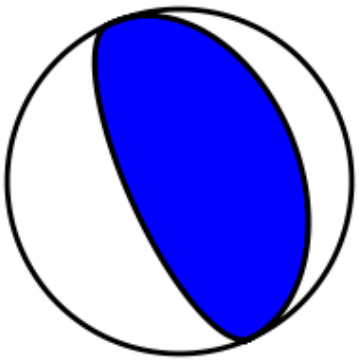

Figure 84: Beach ball for Albania

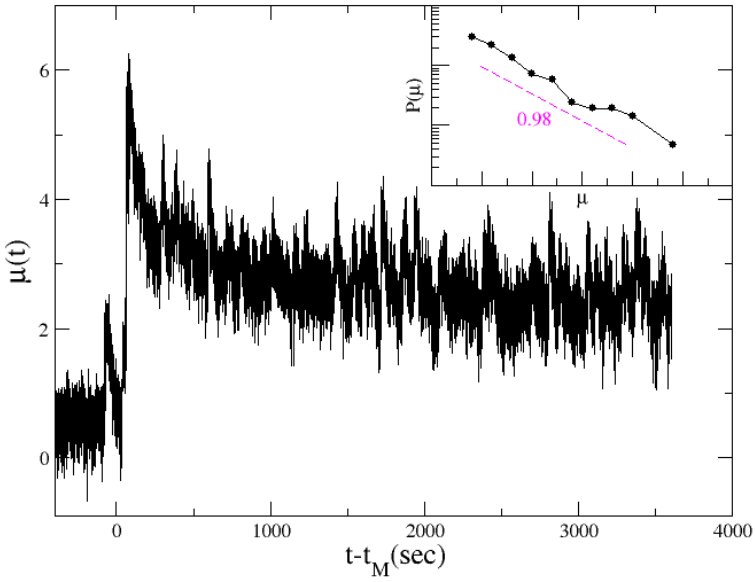

Figure 85: In main panel we plot the envelope function after the Albania earthquake. (Inset) Distribution of the percieved magnitude $P(\mu)$ calculated considering all aftershocks with percieved magnitude $\mu = \mu_M - 3$ in a 24-hours time window after the mainshock occurrence.

The network and the name of the considered seismic station is AC.PHP at coordinates 41.6847N, 20.4408E at altitude 670 m with sampling frequency of 100 Hz.

2.32 PLATANOS 2019/11/27

A Mw6.0 earthquake struck 43 km NW of Platanos, Greece. The event occurred of a depth of about 60 km.

Table 43: W-phase Moment Tensor for Crete 2019

Moment	$1.475E18$ N-m
Magnitude	6.05 Mw
Depth	60.5 km
Half duration	2.62 sec

	Strike	**Dip**	**Rake**
NP1	184°	57°	47°
NP2	63°	52°	136°

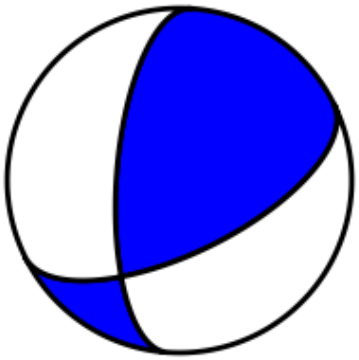

Figure 86: Beach ball for Crete 2019

The network and the name of the considered seismic station is HL.ANKY at coordinates 35.8670N, 23.30117E at altitude 143 m with sampling frequency of 100 Hz.

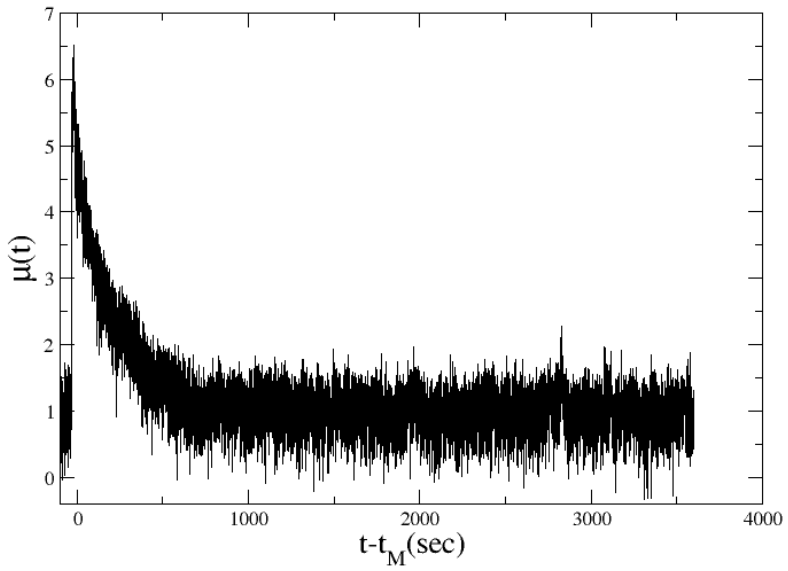

Figure 87: In main panel we plot the envelope function after the Platanos earthquake. We do not plot the distribution of the percieved magnitude $P(\mu)$ because we find only a small number of aftershocks with percieved magnitude $\mu = \mu_M - 3$ in a 24-hours time window after the mainshock occurrence

2.33 PORT HARDY 2019/12/23 - 2019/12/23 - 2019/12/25

Three major earthquakes occurred off west coast of Vancouver Island. The first, a Mw6.0, struck at 19:49 UTC on 2019-12-23. It was 178 km west of Port Hardy at a depth of about 11 km. The second, a Mw6.0, happened at 20:56 on 2019-12-23. It was 166 km southwest of Port Hardy at a depth of about 11 km. The third one, a Mw6.3, struck at 2019-12-25. It was 180 km west of Port Hardy at depth of about 11 km.

Table 44: W-phase Moment Tensor for Port Hardy 2019 foreshock 1

Moment	$1.302E18$ N-m
Magnitude	6.01 Mw
Depth	11.5 km
Half duration	2.63 sec

	Strike	**Dip**	**Rake**
NP1	324°	78°	178°
NP2	54°	88°	12°

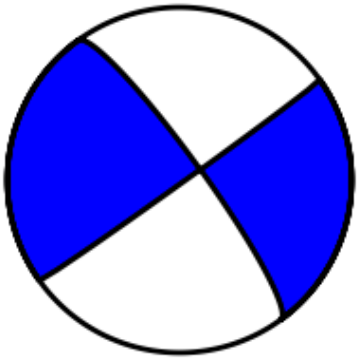

Figure 88: Beach ball for Port Hardy 1

Table 45: W-phase Moment Tensor for Port Hardy 2019 foreshock 2

Moment	$1.337E18$ N-m
Magnitude	6.02 Mw
Depth	11.5 km
Half duration	2.65 sec

	Strike	**Dip**	**Rake**
NP1	46°	83°	−10°
NP2	137°	80°	−173°

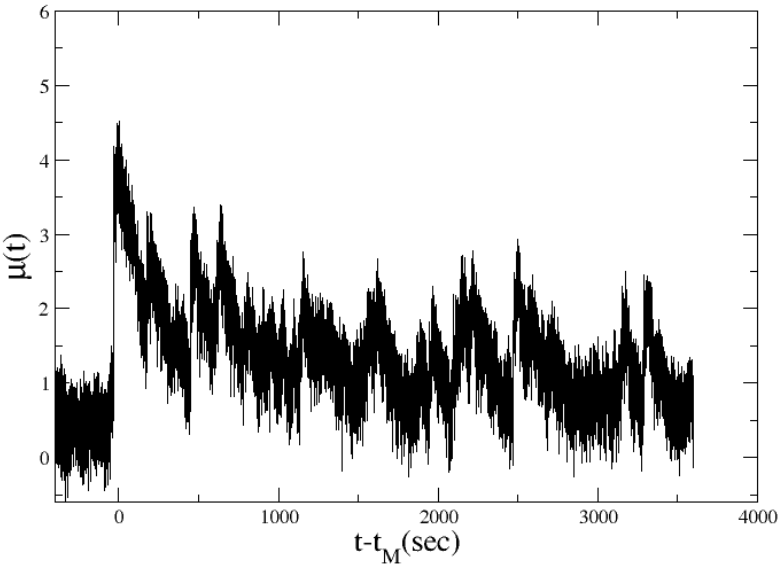

Figure 89: In main panel we plot the envelope function after the Mw6.0 Port Hardy 2019 foreshock. The Distribution of the percieved magnitude $P(\mu)$ calculated considering all aftershocks with percieved magnitude $\mu = \mu_M - 3$ in a 24-hours time window after the mainshock occurrence, substantially coincides with the one plotted in Fig.91.

Table 46: W-phase Moment Tensor for Port Hardy 2019 mainshock

Moment	$3.085E18$ N-m
Magnitude	6.26 Mw
Depth	11.5 km
Half duration	3.49 sec

	Strike	**Dip**	**Rake**
NP1	337°	78°	172°
NP2	69°	82°	12°

The network and the name of the considered seismic station is CN.BBB at coordinates 52.1847N, 128.1133 O at altitude 14 m with sampling frequency of 40 Hz.

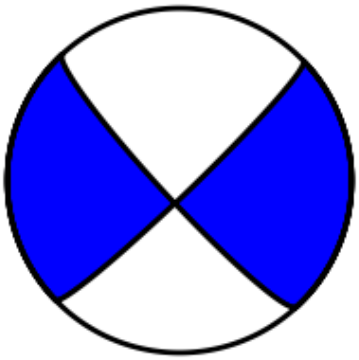

Figure 90: Beach ball for Port Hardy 2

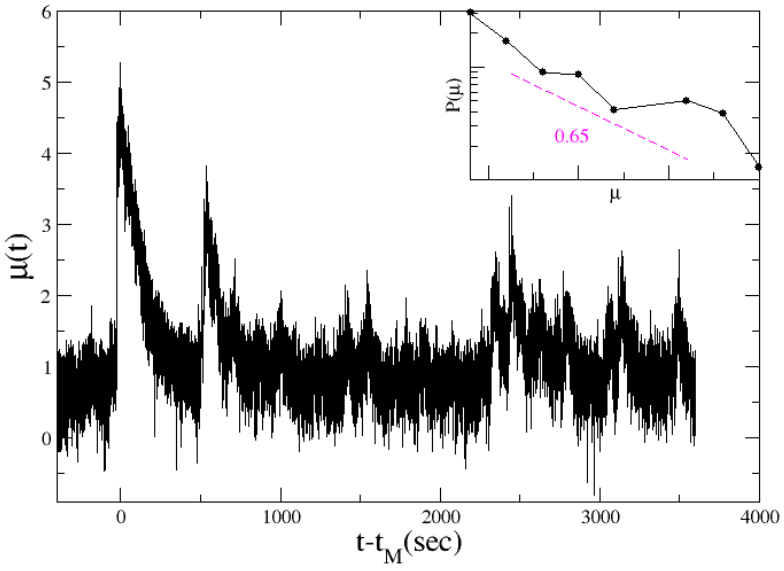

Figure 91: In main panel we plot the envelope function after the Mw6.0 Port Hardy 2019 second foreshock. (Inset) Distribution of the percieved magnitude $P(\mu)$ calculated considering all aftershocks with percieved magnitude $\mu = \mu_M - 3$ in a 24-hours time window after the mainshock occurrence.

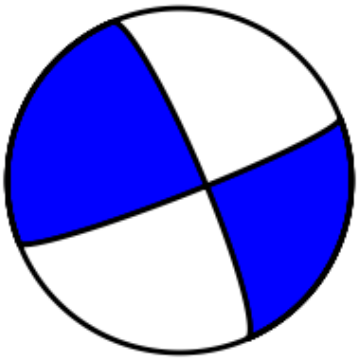

Figure 92: Beach ball for Port Hardy mainshock

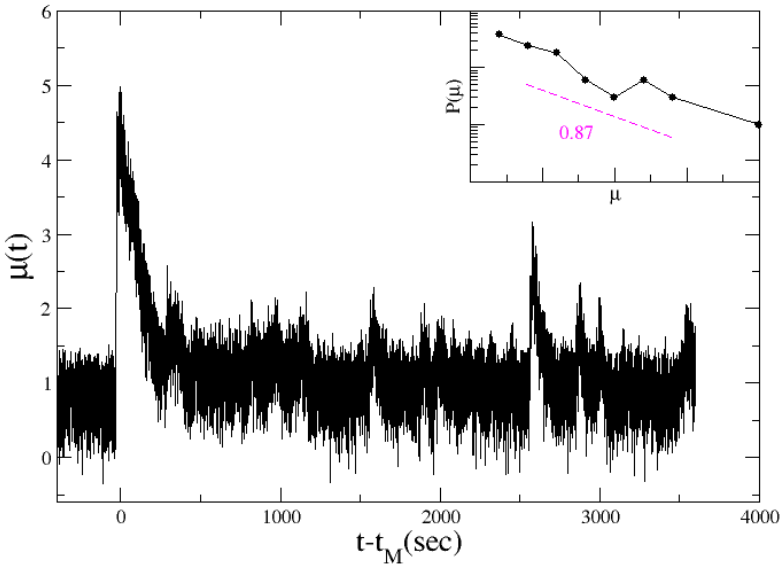

Figure 93: In main panel we plot the envelope function after the Mw6.3 Port Hardy 2019 mainshock. (Inset) Distribution of the percieved magnitude $P(\mu)$ calculated considering all aftershocks with percieved magnitude $\mu = \mu_M - 3$ in a 24-hours time window after the mainshock occurrence.

2.34 IDAHO 2020/03/31

A Mw6.5 earthquake struck 70 km W of Challis, Idaho. The event occurred of a depth of about 19 km.

Table 47: W-phase Moment Tensor for Idaho

Moment	$6.671E18$ N-m
Magnitude	6.48 Mw
Depth	19.5 km
Half duration	4.50 sec

	Strike	**Dip**	**Rake**
NP1	269°	67°	−163°
NP2	172°	74°	−24°

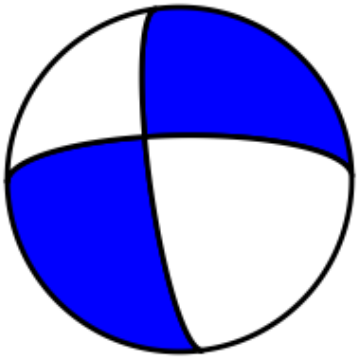

Figure 94: Beach ball for Idaho

The network and the name of the considered seismic station is US.HLID at coordinates 43.5625N, 114.4138 O at altitude 1772 m with sampling frequency of 40 Hz.

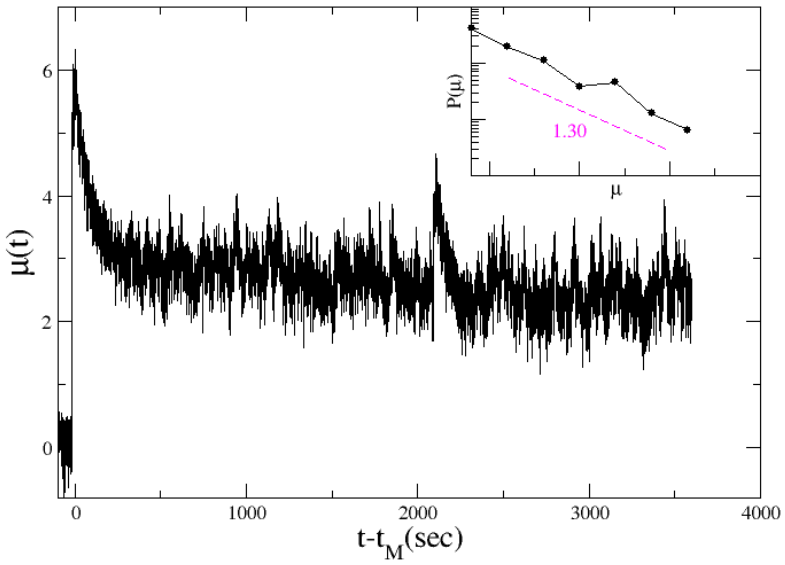

Figure 95: In main panel we plot the envelope function after the Idaho earthquake. (Inset) Distribution of the percieved magnitude $P(\mu)$ calculated considering all aftershocks with percieved magnitude $\mu = \mu_M - 3$ in a 24-hours time window after the mainshock occurrence.

2.35 OFUNATO 2020/04/19

A Mw6.3 earthquake struck 31 km SE of Ofunato, Japan. The event occurred of a depth of about 60 km.

Table 48: W-phase Moment Tensor for Ofunato

Moment	$3.970E18$ N-m
Magnitude	6.33 Mw
Depth	60.5 km
Half duration	3.53 sec

	Strike	**Dip**	**Rake**
NP1	186°	30°	77°
NP2	20°	61°	97°

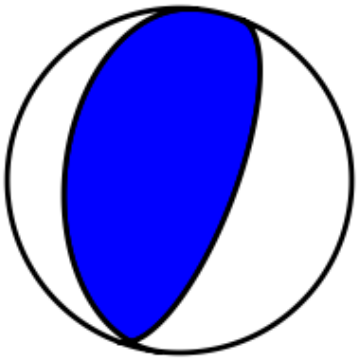

Figure 96: Beach ball for Ofunato

The network and the name of the considered seismic station is N.KKWH at coordinates 38.9207N, 141.6377E at altitude 80 m with sampling frequency of 100 Hz.

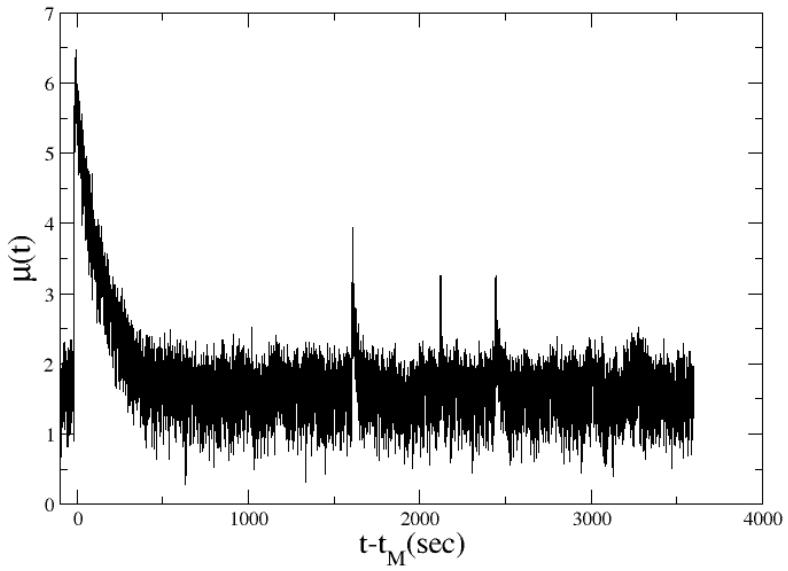

Figure 97: In main panel we plot the envelope function after the Ofunato earthquake. We do not plot the distribution of the percieved magnitude $P(\mu)$ because we find only a small number of aftershocks with percieved magnitude $\mu = \mu_M - 3$ in a 24-hours time window after the mainshock occurrence.